

A Thesis Presented to  
The Faculty of Alfred University

CRYSTALLIZATION OF GLASS FIBERS  
FOR FIREPROOF INSULATION

by

Madeleine N. Flint

In Partial Fulfillment of  
the Requirements for  
The Alfred University Honors Program

May 2017

Under the Supervision of:

Chair: Dr. Scott T. Mixture

Committee Members: Dr. Alexis Clare and Dr. Garrett McGowan

## ACKNOWLEDGMENTS

First and foremost I would like to thank my thesis advisor Dr. Misture. His guidance, depth of knowledge, and encouragement were invaluable. This project further solidified my desire to pursue research, and would not have been possible without him.

I would also like to thank Owens Corning Inc. for providing funds and materials for this research. In particular I would like to thank Becky Skinner and John Hoffman for their mentorship and expertise. Furthermore, I would like to extend my gratitude to Stephanie Maxson for making this project possible.

In addition I would like to extend my thanks to Swavek Zdzieszynski, Gerry Wynick, and Jim Thiebaud for being accessible and accommodating while gathering XRD, SEM, and XPS data. Their contributions were significant and much appreciated.

Lastly, I would like to recognize my family and friends who, throughout my undergraduate career, have given me advice and support. They have always encouraged me to reach my goals and seize every opportunity.

## TABLE OF CONTENTS

	Page
I. Introduction	1
A. Glass-Ceramics	1
B. Glass Wool	4
C. Mineral Wool	5
II. Experimental Procedure	13
A. Differential Scanning Calorimetry (DSC)	13
B. High Temperature X-Ray Diffraction (HTXRD)	13
C. Scanning Electron Microscopy (SEM)	18
D. High Temperature Scanning Electron Microscopy (HTSEM)	18
E. X-Ray Photoelectron Spectroscopy (XPS)	20
III. Results	21
A. DSC	21
B. HTXRD	21
C. SEM	28
D. XPS	30
IV. Discussion	31
A. HTXRD	31
B. SEM	35
C. XPS	37
V. Conclusion	37
VI. Suggestions for Future Work	38
VII. Appendix	39
A. DSC Heat Flow Curves	39
B. Additional SEM Images	43
VIII. References	51

## LIST OF TABLES

Table		Page
I.	Compositions of Three Different Mineral Wools	5
II.	Compositions of Samples A-F	14
III.	$^{\circ}2\theta$ Range of HTXRD Measurements	14
IV.	Temperature Steps & Ramp Rates of Sample A	16
V.	Temperature Steps & Ramp Rates of Sample B	16
VI.	Temperature Steps & Ramp Rates of Sample C	16
VII.	Temperature Steps & Ramp Rates of Sample D	16
VIII.	Temperature Steps & Ramp Rates of Sample E	17
IX.	Temperature Steps & Ramp Rates of Sample F	17
X.	Table X. Tg, Onset of Tc and Peak Tc for Samples A-F in Air and N <sub>2</sub>	21
XI.	Summary Table	36

## LIST OF FIGURES

Figure		Page
1.	Structural schematic of an inosilicate.	3
2.	Structural schematic of a sorosilicate.	4
3.	Structural schematic of a tectosilicates.	4
4.	Mineral wool fibers heat treated at 1000°C for 30 mins.	7
5.	DSC heat flow curve.	9
6.	XRD pattern showing minimal crystallization at 700°C.	9
7.	Relative tensile strength of heat treated mineral wool fibers.	10
8.	Measurement of $\Delta H$ .	11
9.	Mineral wool fibers heat treated for different amounts of time.	11
10.	XRD patterns of a sample heat treated at 860°C for various amounts of time.	12
11.	SEM image of mineral wool fibers heat treated at 860°C.	13
12.	Time-temperature profile of the HTXRD measurements for samples A-F.	15
13.	Time-temperature profile of the HTSEM experiment.	19
14.	HTXRD 3D plot of sample A.	22
15.	HTXRD 3D plot of sample B.	22
16.	HTXRD 3D plot of sample C.	22
17.	HTXRD 3D plot of sample D.	23
18.	HTXRD 3D plot of sample E.	23
19.	HTXRD 3D plot of sample F (air).	23
20.	HTXRD 3D plot of sample F (4% H <sub>2</sub> ).	24
21.	Phase ID of sample A after heat treatment.	25
22.	Phase ID of sample B after heat treatment.	25
23.	Phase ID of sample C after heat treatment.	26
24.	Phase ID of sample D after heat treatment.	26
25.	Phase ID of sample E after heat treatment.	26

26.	Phase ID of sample F after heat treatment (air).	27
27.	Phase ID of sample B after heat treatment (4% H <sub>2</sub> ).	27
28.	Phase ID of sample C at 820°C and 900°C illustrating how originally Ca <sub>2</sub> SiO <sub>4</sub> was present at 820°C, but faded out at 900°C.	27
29.	SE image of sample B heat treated at 800°C for 1 hr.	28
30.	SE image of sample C heat treated at 800°C for 1 hr.	28
31.	SE image of sample D heat treated at 800°C for 1 hr.	29
32.	SE image of sample F heat treated at 800°C for 1 hr.	29
33.	SE images of sample F heated in air and a low pO <sub>2</sub> atmosphere.	30
34.	XPS scan of sample A pre heat treatment.	31
35.	XPS scan of sample A post heat treatment.	31
36.	Sample A- Intensity of Major Peak vs. Temperature.	32
37.	Sample B- Intensity of Major Peak vs. Temperature.	33
38.	Sample C- Intensity of Major Peak vs. Temperature.	33
39.	Sample D- Intensity of Major Peak vs. Temperature.	33
40.	Sample E- Intensity of Major Peak vs. Temperature.	34
41.	Sample F (air)- Intensity of Major Peak vs. Temperature.	35
42.	Sample F (4% H <sub>2</sub> )- Intensity of Major Peak vs. Temperature.	35
43.	Iron content vs. crystal size.	36

## ABSTRACT

Mineral wool is a truly engineered material in that at room temperatures it is a glass, but when heated above the crystallization temperature, it crystallizes. The main application of mineral wool is fireproof insulation, although it also provides thermal and acoustic insulation. When traditional fiberglass insulation is subjected to high temperatures, it slumps or melts. However, when mineral wool insulation is exposed to these elevated temperatures, it crystallizes and is able to maintain its structural integrity. The main focus of this work was to study the nucleation and crystallization behavior of this glass-ceramic. The hypothesis of the study is that iron, in particular iron (II) promotes crystallization. Several methods of characterization were carried out to study the crystallization of this material including Differential Scanning Calorimetry (DSC), High Temperature X-ray Diffraction (HTXRD), High Temperature Scanning Electron Microscopy (HTSEM), SEM, and X-ray Photoelectric Spectroscopy (XPS). Four of the six samples provided by Owens Corning Inc. formed the phase clinopyroxene  $[\text{Ca}(\text{Mg}, \text{Al})((\text{Si}, \text{Al})\text{O}_6)]$ . Akermanite  $[\text{Ca}_2(\text{Mg}, \text{Fe}, \text{Al})(\text{Fe}, \text{Al})\text{Si}_2\text{O}_7]$  was the main phase of the other two samples. Akermanite is classified under the sorosilicates, which form silicon tetrahedral pairs, while clinopyroxene is classified under the inosilicates, which form chains of silicon tetrahedra. Samples with a lower former to modifier ratio formed a sorosilicate because it had more modifier and modifiers tend to break up the glass network. Samples with a higher former to modifier ratio contained fewer modifiers, so they formed long chains of silicon tetrahedra (inosilicates). The nature of nucleation and growth was as expected, as samples with lower iron content contained larger crystals, presumably from fewer nuclei. This trend was observed across an iron content ranging from 2.65 wt% to 17.32 wt%. This research will enable optimizations of their raw materials to provide cost and energy savings in manufacturing.

# **I. Introduction**

## **A. Glass-Ceramics**

Like many scientific discoveries, glass-ceramics were discovered by accident. In 1954, a Corning Inc. chemist by the name of Donald Stookey placed an experimental glass sample in a furnace overnight. He returned in the morning only to discover the furnace had overheated. He expected to find a melted pool of glass inside, but he actually found quite the opposite. An opaque solid with properties much different than a glass or ceramic was sitting inside the furnace. Dr. Stookey accidentally dropped this material, and instead of shattering, it bounced off the floor. Glass-ceramics are now used extensively in material science.<sup>1</sup>

As the name implies, a glass-ceramic is a mixture between a glass and a ceramic. They are formed when a glass is heat treated and undergoes controlled crystallization (devitrification). Materials tend to prefer the crystalline state over a glassy state because it is a lower energy, equilibrium state. First it is important to note that while many glasses are able to form glass-ceramics, not all have this ability. Glasses that are not good candidates for glass-ceramics may be too stable to crystallize. Others may crystallize in a rapid, uncontrollable manner.<sup>2</sup> The crystalline phase usually accounts for 50-95 vol% of the material, while the glassy phase accounts for the rest.<sup>1</sup> One or more crystalline phase, as well as one or more glassy phase can form during heat treatment. Typically, the resulting glassy phase is different than that of the parent glass. The microstructure of glass-ceramics is what makes them a truly unique and useful material.<sup>2</sup>

The crystallization process is a critical part of the formation of a glass-ceramic. This process occurs in two steps, nucleation and growth. Nucleation is the formation of sites for crystals to grow. These submicroscopic nuclei can be formed from transition metals, or other impurities such as dust. The nuclei then grow into larger crystals. As stated above, more than one crystalline phase may form during this process.<sup>2</sup>

The transition of a glass to a glass-ceramic has a significant impact on the properties of the new material. The mechanical properties of a glass-ceramic are much better than those of the parent glass. They have achieved flexural strengths of up to 500 MPa and  $K_{1C}$  toughness values of more than  $3 \text{ MPa}\cdot\text{m}^{1/2}$ . Although these values are still inferior to those of metals, they are far greater than any other translucent material. Glass-ceramics in the  $\text{Li}_2\text{O}-\text{Al}_2\text{O}_3-\text{SiO}_2$  system have a very small coefficient of thermal expansion. Other glass-ceramics have also exhibited near zero thermal expansion behavior. They also have a wide range in optical properties ranging from transparent to opaque to virtually any color. The chemical durability of a glass-ceramic can also vary based on chemical composition of the glassy and crystalline phase. Similar to traditional glasses and ceramics, a glass-ceramic can exhibit insulating electrical properties. However, when combined with other materials such as metals, glass-ceramics can demonstrate high conductivity and even superconductivity. Glass-ceramics are also non-magnetic like traditional glasses or ceramics.<sup>1</sup>

Glass-ceramics formed from silicate parent glasses often form complex silicate crystal structures. The silicon polyhedra have the ability to form isolated tetrahedra (nesosilicates), tetrahedral pairs (sorosilicates), ring silicates (cyclosilicates), chains (inosilicates), layered silicates (phyllosilicates), and network silicates (tectosilicates).<sup>1</sup>

Some of the crystal structures formed during the crystallization of mineral wool fall under the inosilicate category, particularly the single-chain pyroxenes, seen in figure 1 (below)<sup>1</sup>. These chains are linked by  $Mg^{2+}$ ,  $Ca^{2+}$ , or  $Fe^{2+}$ .<sup>3</sup> The silicon to oxygen ratio of these silicates is 1:3. Some common pyroxenes include diopside ( $CaMgSi_2O_6$ ), and augite ( $[(Ca,Na)(Mg,Fe,Al)(Al,Si)_2O_6]$ ).<sup>1</sup>

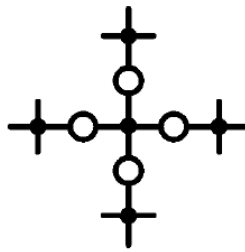


*Figure 1. Structural schematic of an inosilicate.<sup>1</sup>*

Mineral wool can also crystallize as a sorosilicate, seen in figure 2 (below). They have a low Si:O ratio of 2:7. Because of this, they are not usually glass-forming minerals. Sorosilicates are often times present in slag-based glass-ceramics in the form of akermanite ( $Ca_2MgSi_2O_7$ ).<sup>1</sup>

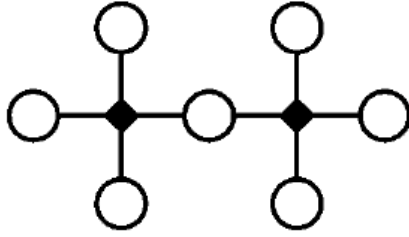


*Figure 2. Structural schematic of a sorosilicate.<sup>1</sup>*

Tectosilicates, or framework silicates are most common network glass-ceramics form. A ball and stick model of a tectosilicates can be seen in figure 3 (below). Their high Si:O ratio of 1:2 makes them ideal. Because they have high glass former content ( $\text{SiO}_2$ ,  $\text{Al}_2\text{O}_3$ ), they almost always form glasses. Nepheline  $\text{Na}_7(\text{Al, Si, O})$  is a common phase found in mineral wool glass-ceramics.<sup>1</sup>

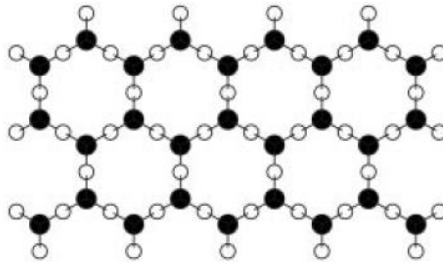


*Figure 3. Structural schematic of a tectosilicates.<sup>1</sup>*

## **B. Glass Wool**

Glass fibers can be separated into two categories: continuous and discontinuous. Continuous glass fiber is formed when the melt is continuously drawn from a source. These glasses are typically used for optical communication and reinforcement of materials. Discontinuous fibers are often formed through a spinning process. Glass wool falls under the discontinuous category.<sup>4</sup> This material is often used for thermal and acoustic insulation.<sup>5</sup>

### C. Mineral Wool

Mineral wool, also known as stone wool, differs from traditional glass wool in its ability to crystallize when exposed to high temperatures. When traditional fiberglass insulation is subjected to high temperatures, it slumps or melts. However, when mineral wool insulation is exposed to these elevated temperatures, it crystallizes and is able to maintain its structural integrity. The crystallization process of these glass fibers is critical, because it changes the physical and chemical properties as well as the microstructure of the material.<sup>6</sup> This is particularly important in the case of a fire where the insulation could potentially see temperatures of 1000°C.<sup>7</sup>

Mineral wool can be made from slag, basalt, and/or, other naturally occurring rocks. Slag is a byproduct of the steel and iron-making industries, meaning much of the final product is made from recycled material.<sup>6</sup> Traditionally, the raw materials are then melted in a copula at around 1425°C, and then spun into fibers. The fibers are alumino-silicate glasses with a significant amount of alkaline earth modifier, some alkali modifier, and a relatively large amount of iron and other transition metals when compared to traditional glasses.<sup>8</sup> Three different mineral wool compositions can be seen below in table I.

*Table I. Compositions of Three Different Mineral Wools<sup>8</sup>*

	SiO <sub>2</sub>	Al <sub>2</sub> O <sub>3</sub>	Fe <sub>2</sub> O <sub>3</sub> <sup>a</sup>	TiO <sub>2</sub>	CaO	MgO	Na <sub>2</sub> O	K <sub>2</sub> O	Other
F1	44.7	13.5	3.3	1.3	16.1	18.7	1.7	0.6	0.1
F2	42.8	12.2	3.3	1.2	24.8	12.9	1.9	0.7	0.2
F3	47.8	16.1	2.7	0.6	18.4	3.2	6.4	4.2	0.6

<sup>a</sup> All iron is reported as Fe<sub>2</sub>O<sub>3</sub>. The ratio [Fe<sup>2+</sup>]/[Fe<sub>tot</sub>] is ~0.35 for F3, whereas no Fe<sup>3+</sup> could be detected in F1 and F2.

Lastly, the fibers are formed into the final product. Mineral wool has been used in acoustic panels, paint and filler, building and firewall insulation, industrial board, blanket, and pipe insulation.<sup>9</sup>

To be considered a fireproof material the mineral wool fibers must have excellent high temperature stability (HTS). This means the geometric shape must remain constant throughout heat treatment. Previous work has show that the atmosphere plays a large role in the high temperature stability of the glass-ceramic fibers. When the fibers were heat treated in an oxidizing atmosphere at around 1000°C, the shape and flexibility remained relatively unchanged. However, when the mineral wool fibers were heat treated in a reducing atmosphere, they sintered. The shape of the fiber changes, and they became hard and brittle.<sup>8</sup>

The oxidation of  $\text{Fe}^{2+}$  to  $\text{Fe}^{3+}$  plays a large role in how the fibers will eventually crystallize. One theory is that the oxidizing process starts out with iron reacting with the atmospheric oxygen in contact with the surface. This creates electron holes as iron changes oxidation states from  $\text{Fe}^{2+}$  to  $\text{Fe}^{3+}$ . To balance the charge on the surface, divalent cations, particularly  $\text{Mg}^{2+}$ , diffuse from the bulk to the surface of the fiber. Magnesium also reacts with oxygen and forms a nano-crystalline layer of MgO at the surface. It is believed that the formation of MgO also layer shifts the onset of crystallization to a lower temperature.<sup>8</sup>

Aside from partaking in the initial crystallization of the stone wool fibers, it is also thought that MgO also plays a large role in maintaining the structural integrity.

The three different samples were heat treated in air at 1000°C for 30 mins, and then analyzed using scanning electron microscopy (SEM). The specimen with the most amount of magnesium maintained the same geometry and had less cracking. The backscattered and secondary electron images can be seen below in figure 4.<sup>8</sup>

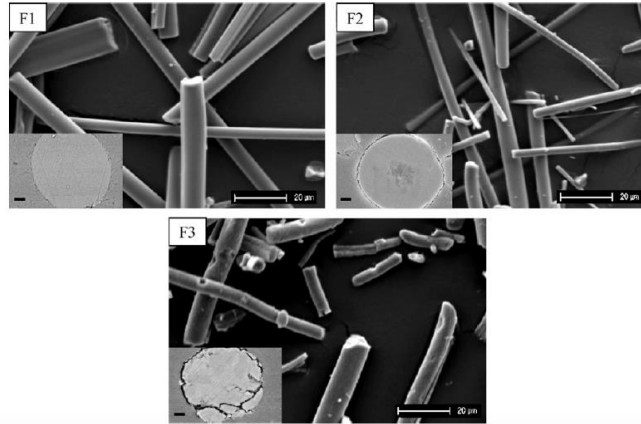


*Figure 4. Mineral wool fibers heat treated at 1000°C for 30 mins. The cross sections were done in backscattered mode, while the fibers were captured in secondary mode.<sup>8</sup>*

This study concluded that a higher initial content of  $\text{Fe}^{2+}$  and  $\text{Mg}^{2+}$  increased the high temperature stability of the fibers. The higher content caused the formation of a larger nano-layer of surface crystals. They also found that the atmosphere in which the alumino-silicate fibers are heat treated in played a large role in the high temperature stability. Heat treating the fibers in atmospheric air caused the oxidation of  $\text{Fe}^{2+}$  to  $\text{Fe}^{3+}$ , and increased the HTS. When fibers were heat-treated in argon or  $\text{H}_2/\text{N}_2$  atmospheres the HTS was lower because of the smaller  $\text{Mg}^{2+}$  and  $\text{Fe}^{2+}$  nano-crystalline layer. Fortunately, if the mineral wool insulation were to encounter a fire, it would most likely be in ambient air, but the data and

results gives valuable information on the importance of iron oxidation state and crystallization.<sup>8</sup>

Another study found similar results that an increase in the  $\text{Fe}^{2+}/\text{Fe}^{3+}$  ratio increased the rate of crystallization, however their reasoning was slightly different. The study found that magnetite and pyroxene content was lower in heat treated powder samples than in heat treated bulk samples. Surface oxidation had a negative effect on magnetite formation. Since the powdered samples to had more surface area, less magnetite formed when compared to the bulk samples. As a result pyroxene content also decreased, because pyroxene was formed by a reaction between magnetite and the glass.<sup>3</sup>

$\text{Mg}^{2+}$  and  $\text{Fe}^{2+}$  played an important role in linking the chains on silicon tetrahedra. Oxidation of the surface layer lead to the migration of iron from the bulk to the surface, decreasing the amount of  $\text{Fe}^{2+}$  that was able to link pyroxene chains. The amount of  $\text{Fe}^{2+}$  was then increased in a new batch by the addition of carbon. The powder and bulk samples were then heat treated again. The total crystallization rate and magnetite formation increased, while the amount of pyroxene and total crystal phase formed decreased.<sup>3</sup>

Another study done in China analyzed the crystallization behavior of mineral wool. They found that according to differential scanning calorimetry measurements (DSC) the onset of crystallization temperature was  $854^{\circ}\text{C}$ , however there was minimal crystallization found at  $700^{\circ}\text{C}$  according to the x-ray diffraction (XRD) patterns.<sup>6</sup> This discrepancy could be partially due to the different thermal histories

the fibers experienced. Figures 5 and 6 (below) show the DSC heat flow curve, and XRD patterns respectively.

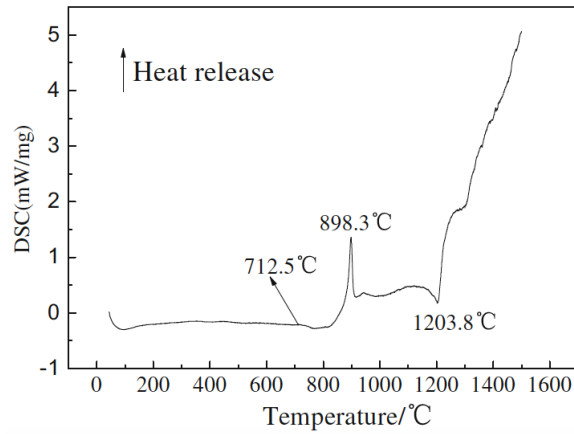


Figure 5. DSC heat flow curve depicting a  $T_g$  at 712.5°C, onset of crystallization at around 845°C peak crystallization at 898.3°C, and a melting temperature at 1203.8°C.<sup>6</sup>

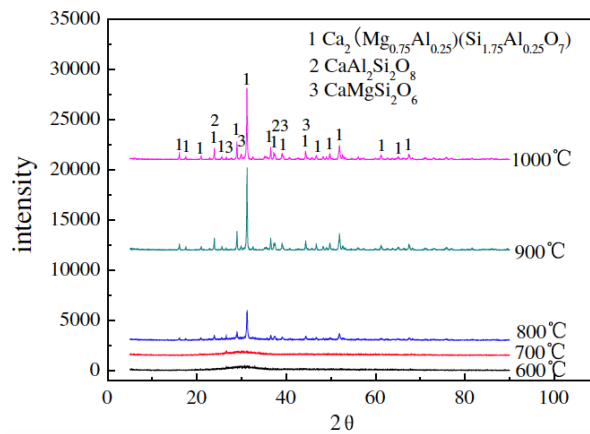
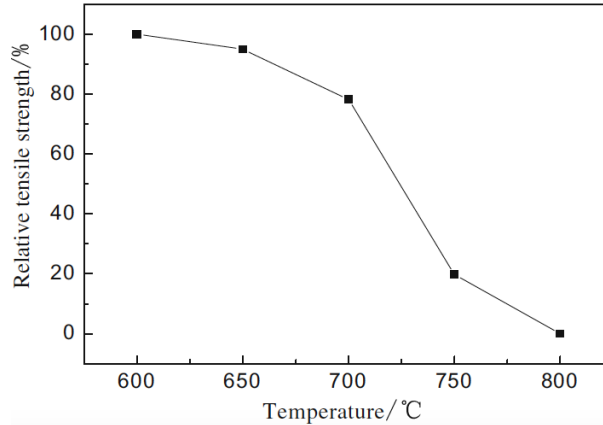


Figure 6. XRD pattern showing minimal crystallization at 700°C.<sup>6</sup>

The study also found that the sample crystallized faster at a higher temperature. Although the fibers crystallized faster at higher temperatures, the strength decreased with an increase in temperature. The decrease in strength started out slow, but increased as the heat treatment temperature increased. At 650°C the material retained 95% of its strength, while at 750°C the mineral wool

fibers retained only about 20% of its original strength. Above 800°C the fibers become too brittle to be subjected to tensile force. This can be seen in figure 7 (below).<sup>6</sup>



*Figure 7. Relative tensile strength of heat treated mineral wool fibers.<sup>6</sup>*

This particular study also found that diopside ( $\text{CaMgSi}_2\text{O}_6$ ) was the first phase to form. Over time other phases grew in rapidly, but the amount of diopside remained relatively constant.<sup>6</sup>

Another study measured the relative degree of crystallization using several different methods. DSC heat flow curves were used to measure the heat flow ( $\Phi$ ) of a material upon a temperature change. The change in enthalpy ( $\Delta H$ ) was also measured by finding the area under the curve of the crystallization peak, or the integration seen in figure 8 (below).<sup>10</sup>

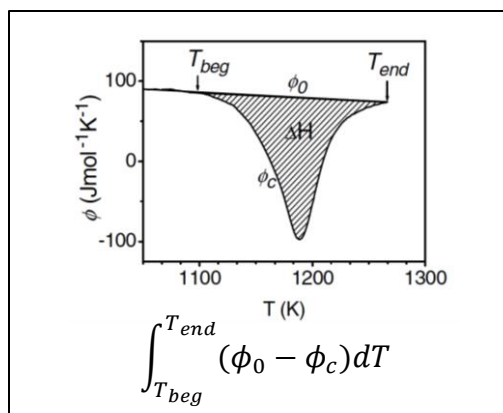


Figure 8. Measurement of  $\Delta H$ .  $T_{beg}$  is the temperature at which the exothermic crystallization peak begins,  $T_{end}$  is the temperature at which the peak ends,  $\Phi_0$  is an approximated linear curve going from  $T_{beg}$  to  $T_{end}$ ,  $\Phi_c$  is the heat flow curve.<sup>10</sup>

It is important to note that thermal properties of the material vary based on the thermal history, so consistency throughout experimentation was crucial. A sample of crushed fiber was measured in the DSC pre heat treatment to obtain  $\Delta H_0$ . Insulation was then heat treated at different temperatures for various durations, and ground into powders. The process described in Figure 9 was then repeated for samples such as those in Figure Y (below) to obtain  $\Delta H_{ht}$ . The degree of crystallinity was then determined by the formula:  $\Delta H_{ht}/\Delta H_0$ .<sup>10</sup>

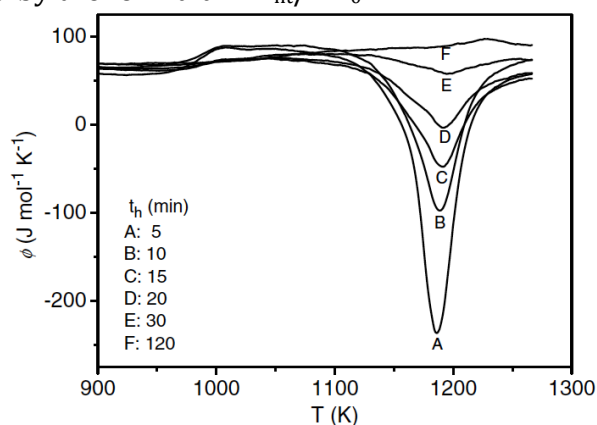
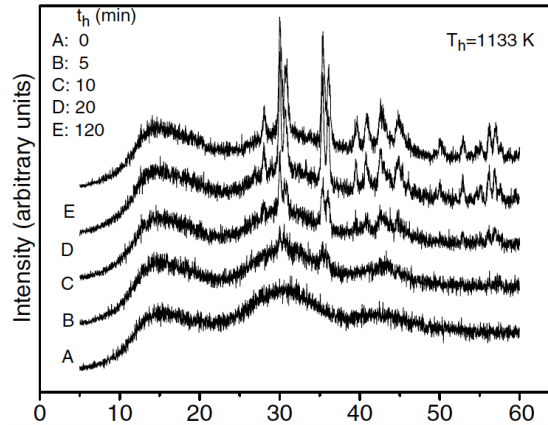


Figure 9. Mineral wool fibers heat treated for different amounts of time.<sup>10</sup>

Similarly to DSC, the amount of crystallization can also be determined through use of XRD. The same powders that were used for DSC measurements can be used to gather X-ray patterns such as those seen in figure 10 (below). By means of Rietveld refinement the total amount of crystalline and amorphous phase can be determined.<sup>10</sup>



*Figure 10. XRD patterns of a sample heat treated at 860°C for various amounts of time.<sup>10</sup>*

Unlike the first two techniques, the last method for determining the degree of crystallinity is more qualitative. Cross sections of the fibers were analyzed with a SEM to determine the relative degree of crystallization. The fibers observed in Figure 11 (below) were examined using back-scattered electrons. The dark area represented the amorphous phase, and the light area represented the crystalline phase. This technique can only be used if there is a large compositional contrast between the two phases. If the amorphous and crystalline phase have similar compositions, this method cannot be used.<sup>10</sup>

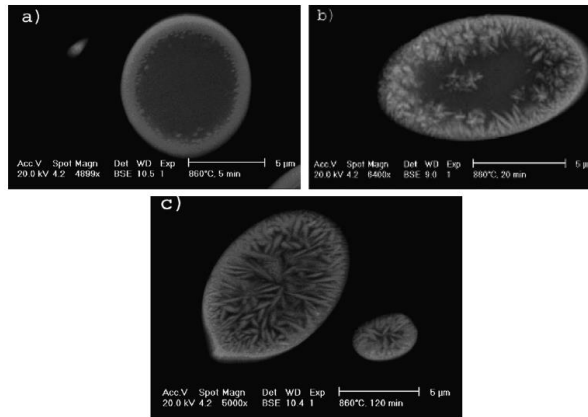


Figure 11. SEM image of mineral wool fibers heat treated at 860°C for a) 5 mins, b) 20 mins, and c) 120 mins.<sup>10</sup>

## II. Experimental Procedure

### A. Differential Scanning Calorimetry (DSC)

Differential Scanning Calorimetry (DSC) was used to gain thermal information about samples A-F. About 20mg of fine powder were placed in an alumina crucible inside of a TA SDTQ600 DSC. The DSC scans went from 25°C to 1275°C at a rate of 20°C/min. Each sample was tested in both air and N<sub>2</sub> atmospheres. The glass transition temperature, onset of crystallization temperature, and peak crystallization temperature were all determined using TA Advantage software.

### B. High Temperature X-ray Diffraction (HTXRD)

High Temperature X-ray Diffraction (HTXRD) was used to analyze phases and observe crystallization in samples A, B, C, D, E, and F. The compositions of

samples A-F can be seen below in table II. They are arranged in order of decreasing iron content.

*Table II. Compositions of Samples A-F*

<b>Sample</b>	<b>A</b>	<b>B</b>	<b>C</b>	<b>D</b>	<b>E</b>	<b>F</b>
SiO <sub>2</sub> (wt%)	46.48	47.7	40.99	40.12	44.27	44.03
CaO (wt%)	10.74	11.71	27.79	21.02	22.67	29.54
Al <sub>2</sub> O <sub>3</sub> (wt%)	11.79	16.41	9.55	18.18	12.24	10.64
MgO (wt%)	6.86	6.77	8.33	7.95	8.37	9.44
<b>Total Fe (wt%)</b>	<b>17.32</b>	<b>11.45</b>	<b>8.93</b>	<b>7.13</b>	<b>7.08</b>	<b>2.65</b>
Fe <sub>2</sub> O <sub>3</sub> (wt%)	8.72	4.98	4.04	2.059	3.54	0.725
FeO (wt%)	7.9	5.83	4.40	4.5	3.19	1.732

Samples were received as blocks of insulation. They were ground into a fine powder using a mortar and pestle. Isopropanol was added to the powder to get a thin, even layer on top of the sapphire sample holder. The sample holder was then placed in a Siemens D5000 diffractometer. This instrument contained a custom XRD furnace.<sup>11</sup> The specimens were measured in ambient air, and cobalt radiation was used to collect the data. The range of  $2\theta$  in which each sample was measured can be found in table III (below).

*Table III.  $2\theta$  Range of HTXRD Measurements*

Sample Name	Start Position ( $^{\circ}2\theta$ )	End Position ( $^{\circ}2\theta$ )
A	10	75
B	15	60
C	15	60
D	15	60
E	15	65
F (Air)	15	60
F (4% H <sub>2</sub> )	10	55

The data for each sample was captured using a step size of  $0.03^{\circ}2\theta$  with a 0.5s count time. The time-temperature profiles and temperature steps for each sample as well as ramp rates can be found in figure 12 tables and IV-IX (below) respectively. Temperature steps varied from sample to sample, but were kept consistent with respect to their thermal properties. The first high temperature measurement was taken just before the glass transition temperature. The instrument started taking XRD measurements at increments of  $10^{\circ}\text{C}$  just before the onset of crystallization temperature, and continued past the peak crystallization temperature. HTXRD measurements were taken at the end of each temperature step. Each sample was also measured before and after heat treatment at room temperature. The phase ID as well as the creation of 3D HTXRD plots was done using Jade MDI software. Time-temperature profiles, and intensity of major peaks vs. temperature plots were made using Microsoft Excel.

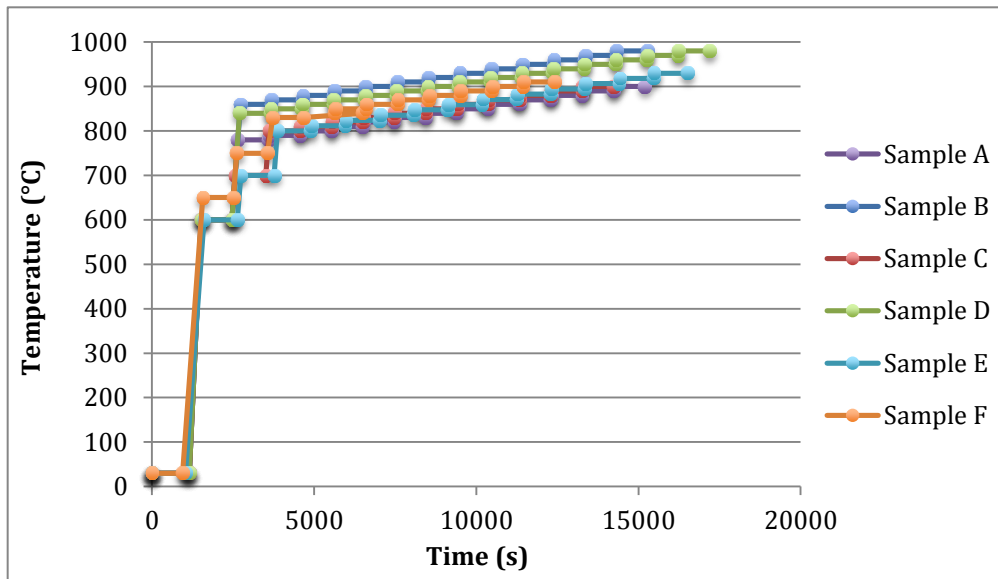


Figure 12. Time-temperature profile of the HTXRD measurements for samples A-F.

*Table IV. Temperature Steps & Ramp Rates of Sample A*

T <sub>i</sub> (°C)	T <sub>f</sub> (°C)	Temperature Increase per Step (°C)	Ramp Rate (°C/s)
30	600		1
600	780		1
780	900	10	0.5
900	30		

*Table V. Temperature Steps & Ramp Rates of Sample B*

T <sub>i</sub> (°C)	T <sub>f</sub> (°C)	Temperature Increase per Step (°C)	Ramp Rate (°C/s)
30	600		1
600	860		1
860	980	10	0.5
980	30		

*Table VI. Temperature Steps & Ramp Rates of Sample C*

T <sub>i</sub> (°C)	T <sub>f</sub> (°C)	Temperature Increase per Step (°C)	Ramp Rate (°C/s)
30	600		1
600	700		1
700	800		1
800	900	10	0.5
900	30		

*Table VII. Temperature Steps & Ramp Rates of Sample D*

T <sub>i</sub> (°C)	T <sub>f</sub> (°C)	Temperature Increase per Step (°C)	Ramp Rate (°C/s)
30	600		1
600	840		1
840	980	10	0.5
980	30		

*Table VIII. Temperature Steps & Ramp Rates of Sample E*

T <sub>i</sub> (°C)	T <sub>f</sub> (°C)	Temperature Increase per Step (°C)	Ramp Rate (°C/s)
30	600		1
600	700		1
700	800		1
800	980	10	0.5
980	30		

*Table IX. Temperature Steps & Ramp Rates of Sample F*

T <sub>i</sub> (°C)	T <sub>f</sub> (°C)	Temperature Increase per Step (°C)	Ramp Rate (°C/s)
30	650		1
650	750		1
750	830		1
830	910	10	0.5
900	30		

Sample F was also analyzed in a 4% hydrogen/ 96% nitrogen atmosphere. The flow rate of hydrogen was held constant throughout the entirety of the experiment at 200 mL/min. Sample prep was similar to the other HTXRD experiment but used an Anton Paar HTK1200 furnace. The block of insulation was crushed into a fine powder using a mortar and pestle, and then placed in an Anton Paar sample holder. The sample was then placed in a Bruker D8 Advance diffractometer, and was measured using Cu K $\alpha$  radiation. The data for this sample was captured using the same step size of 0.03°2 $\theta$  with a 0.5s count time. The temperature profile is the same as that of the sample tested in air, however the range of °2 $\theta$  in which the sample was measured was shifted 5°2 $\theta$  to account for the

different radiation used. This can be seen in table I (above). Analysis of the data was done in Jade software.

### **C. Scanning Electron Microscopy (SEM)**

Scanning electron microscopy (SEM) was used to observe the glass fibers before heat treatment, and crystal size and morphology after heat treatment. Samples A through F were analyzed before and after heat treatment. All samples were heat treated in air at 800°C for 1 hour. The residue from the inside of the sample holder was mounted to double-stick carbon tape that was then placed on a larger metal sample holder. A JEOL SEM was used in secondary electron mode with an Everhart-Thornley detector to capture the images. An accelerating potential of 2.00kV and a working distance of 4.0mm were used for most of the images, but were adjusted if necessary. All samples were imaged at 5,000X, 20,000X, and 50,000X. If there was a particular surface feature that was deemed important, the magnification was adjusted accordingly.

### **D. High Temperature Scanning Electron Microscopy (HTSEM)**

High temperature scanning electron microscopy (HTSEM) was also performed to visually observe the crystallization process. Sample F had the largest crystals, so it was chosen for this experimentation. The block of insulation was crushed into a fine powder using a mortar and pestle. It was then mixed with isopropanol, and a very small amount was placed on a protochip. The protochip provided a platform for the rapid heat treatment of the sample. An optical microscope was used to ensure there were fibers on the area that was to be heated.

This was confirmed when the protochip was placed in the same JEOL SEM and imaged at 1,000X. The sample was heated in low vacuum mode to get as much oxygen in the chamber as possible. The pressure started out at 128Pa, but was increased to 170Pa 45mins into the experiment. The sample was heated at a rate of 400°C/min from room temperature to 750°C. The temperature was then held constant at 750°C for 5mins to allow the fibers to fully come to temperature. The temperature then increased to 825°C and was held constant for over two hours. A time-temperature curve for this experiment can be seen in figure 13 (below).

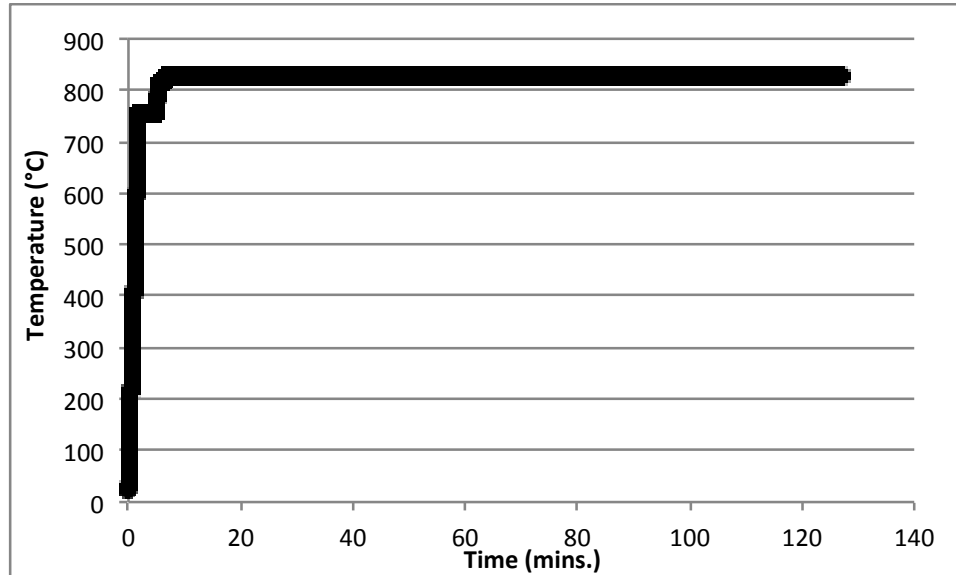


*Figure 13. Time-temperature profile of the HTSEM experiment.*

The images taken before and after heat treatment were taken in secondary mode. The movie and any images taken during heat treatment were captured in back-scattered electron mode. An Everhart-Thornley detector was used for secondary electrons, while a solid-state detector was used for back-scattered

electrons. Most of the images were captured using an accelerating potential of 2.00kV and a working distance of 4.0mm, but were adjusted if necessary. The magnification ranged from 150X to 100,000X depending on the morphology and fiber being observed.

### **E. X-ray Photoelectron Spectroscopy (XPS)**

X-ray photoelectron spectroscopy (XPS) was used to obtain information about the iron oxidation states. Powdered samples on the high (A) and low (F) end of the iron ranges were chosen for experimentation. In total there were four samples analyzed; sample A pre and post heat treatment as well as sample F pre and post heat treatment. The samples were measured in a PHI Quanta SXM with an aluminum X-ray source. The beam power was set at 25kW and 15kV with a 100 $\mu$ m beam size. A multi-channel analyzer was used to detect the x-rays coming off the samples. The pressure of the chamber was  $1 \times 10^{-9}$  torr. A low-resolution survey scan was performed using a pass energy of 224eV, a step size of 0.4eV, and a time per step of 20ms. A high-resolution scan was then done around the iron peaks using a pass energy of 26eV, a step size of 0.05eV, and a time per step of 20ms. Each specimen was measured five times. A neutralizer was also used because of the insulating nature of these materials. A neutralizer uses a low energy electron gun and a low energy ion gun. Analysis of the data was performed in Multi-Pack software.

### III. Results

#### A. DSC

A complete list of T<sub>g</sub>, onset of T<sub>c</sub>, and peak T<sub>c</sub> in air and N<sub>2</sub> can be seen in table X (below). DSC heat flow curves for samples A-F in N<sub>2</sub> and air are located in the appendix. Samples containing a higher iron content had a lower glass transition temperature. Iron does not appear to have an impact on crystallization temperatures.

*Table X. T<sub>g</sub>, Onset of T<sub>c</sub> and Peak T<sub>c</sub> for Samples A-F in Air and N<sub>2</sub>*

Sample	T <sub>g</sub> (°C)		Onset T <sub>c</sub> (°C)		Peak T <sub>c</sub> (°C)	
	Air	N <sub>2</sub>	Air	N <sub>2</sub>	Air	N <sub>2</sub>
A	642	640	831	807	853	825
B	659	645	902	892	936	927
C	688	690	828	827	911	853
D	694	687	870	861	942	908
E	692	681	841	846	922	881
F	727	723	899	850	922	899

#### B. HTXRD

3-D HTXRD plots of samples A-F can be seen in figures 14-20 (below). These plots illustrate how the stone wool samples crystallized as the temperature increased.

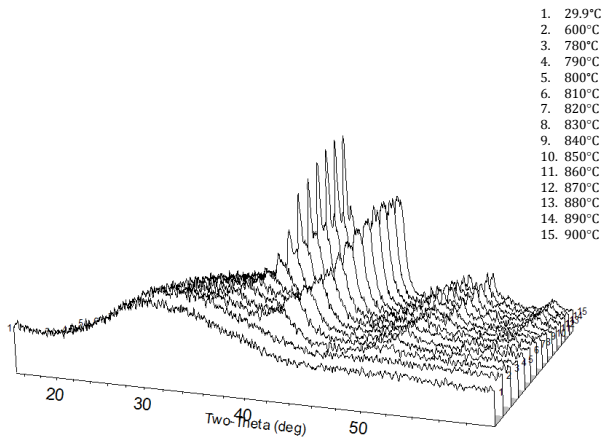


Figure 14. HTXRD 3D plot of sample A.

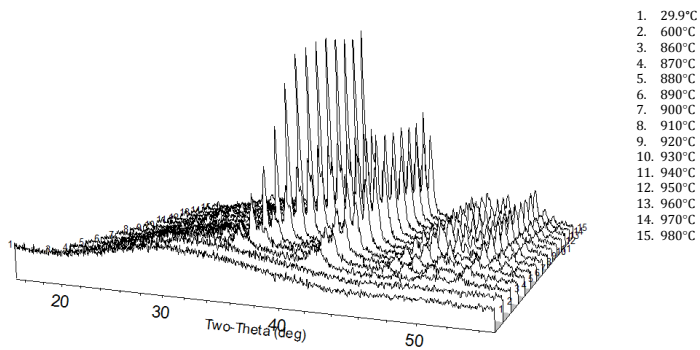


Figure 15. HTXRD 3D plot of sample B.

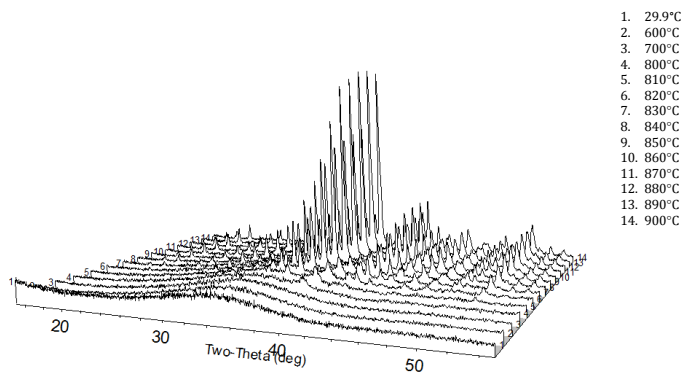


Figure 16. HTXRD 3D plot of sample C.

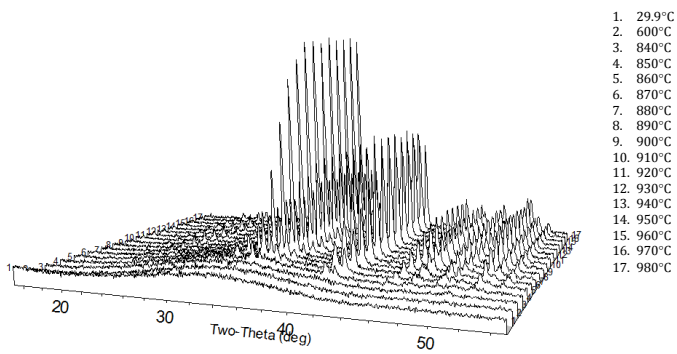


Figure 17. HTXRD 3D plot of sample D.

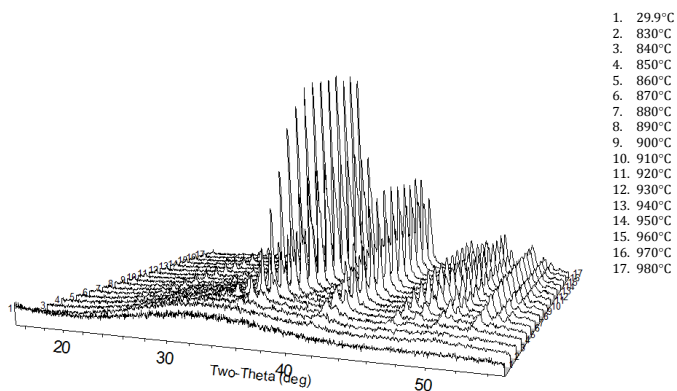


Figure 18. HTXRD 3D plot of sample E.

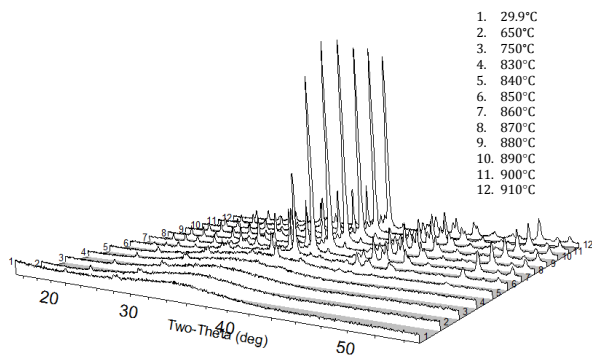
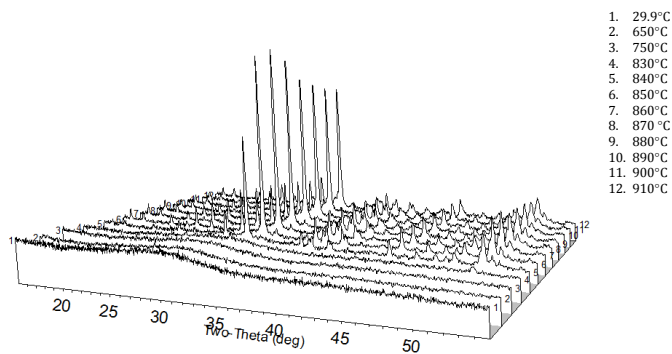


Figure 19. HTXRD 3D plot of sample F (air) using Co radiation. Compare to figure 20, note different radiation.



*Figure 20. HTXRD 3D plot of sample F (4% H<sub>2</sub>) using Cu K $\alpha$  radiation. Compare to figure 19, note different radiation.*

The crystallization of these fibers produced complex crystal phases. Samples A, B, D, and E contained a major phase of clinopyroxene [Ca(Mg,Al)((Si, Al)O<sub>6</sub>)], while samples C and F contained mostly akermanite [Ca<sub>2</sub>(Mg, Fe, Al)(Fe, Al)Si<sub>2</sub>O<sub>7</sub>]. Iron was not included in the chemical formula of clinopyroxene, however Fe<sup>3+</sup> could sit on the Al<sup>3+</sup> lattice site. Samples A, B and E did not contain a minor phase. Sample C contained a minor phase of augite [FeCa<sub>4</sub>Si<sub>8</sub>Mg<sub>2.96</sub>O<sub>24</sub>], and calcium silicate [Ca<sub>2</sub>SiO<sub>4</sub>]. Calcium silicate was the first phase in sample C to appear during heat treatment, but over time, it faded out as the other phases grew in. Sample D contained minor phases of nepheline [Na<sub>7</sub>(Al, Si, O)], and aluminum oxide [MgO]. Sample F also had a minor phase of diopside [Ca(Mg,Al)(Si,Al)<sub>2</sub>O<sub>6</sub>]. Heat treatment of sample F in 4%H<sub>2</sub>/96%N<sub>2</sub> did not appear to have an effect on the phase ID during the HTXRD trials. Phase ID for samples A-F can be seen in figures 21-27 below. These XRD scans were taken after the fibers went through heat treatment and were cooled

down to 30°C. Figure 28. shows the  $\text{Ca}_2\text{SiO}_4$  phase in sample C at 820°C, and how it disappeared in the 900°C scan.

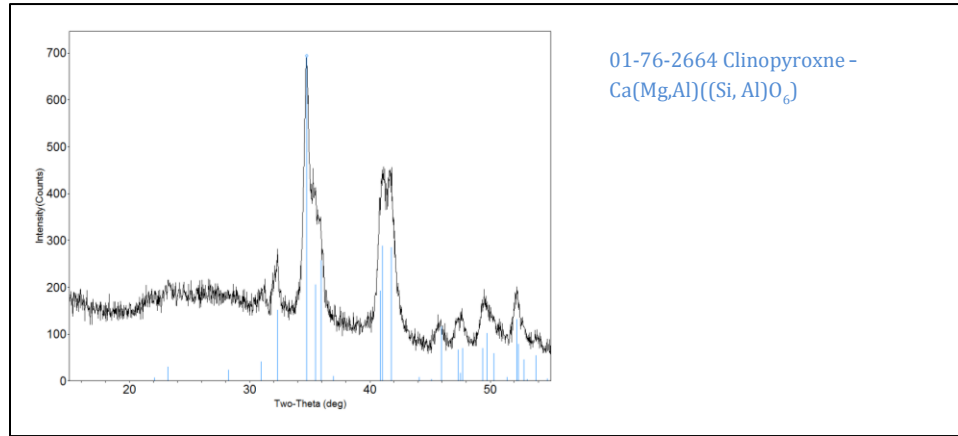


*Figure 21. Phase ID of sample A after heat treatment.*

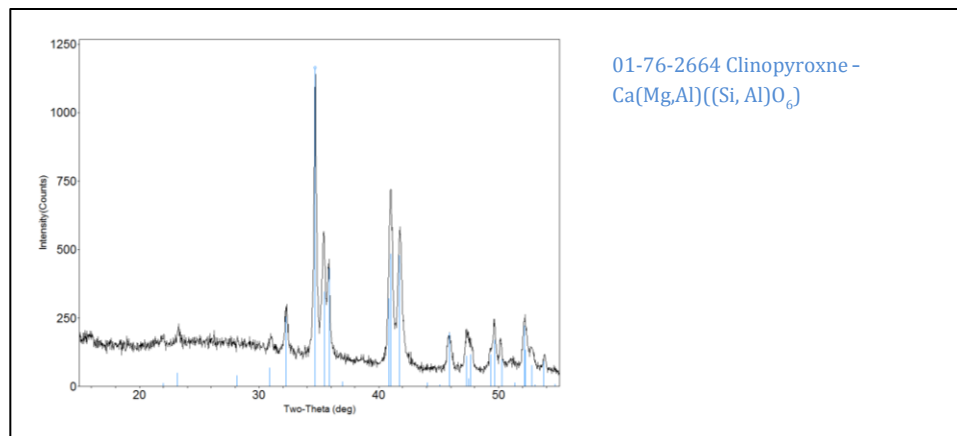


*Figure 22. Phase ID of sample B after heat treatment.*

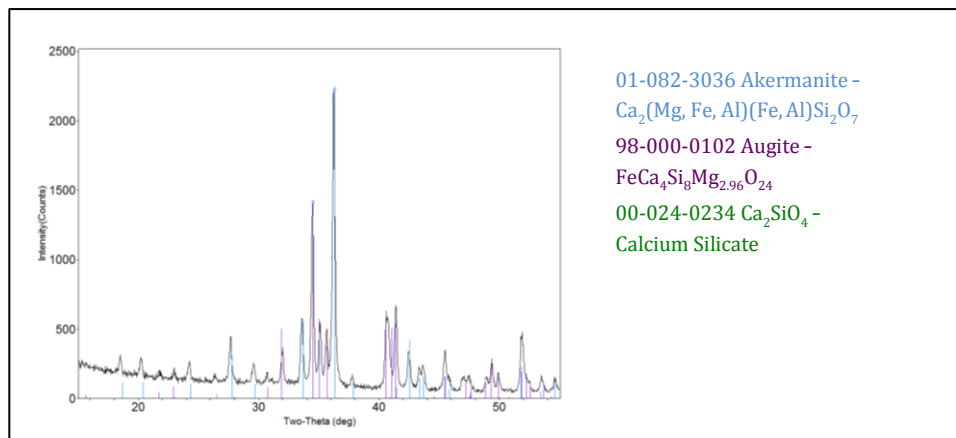


Figure 23. Phase ID of sample C after heat treatment.

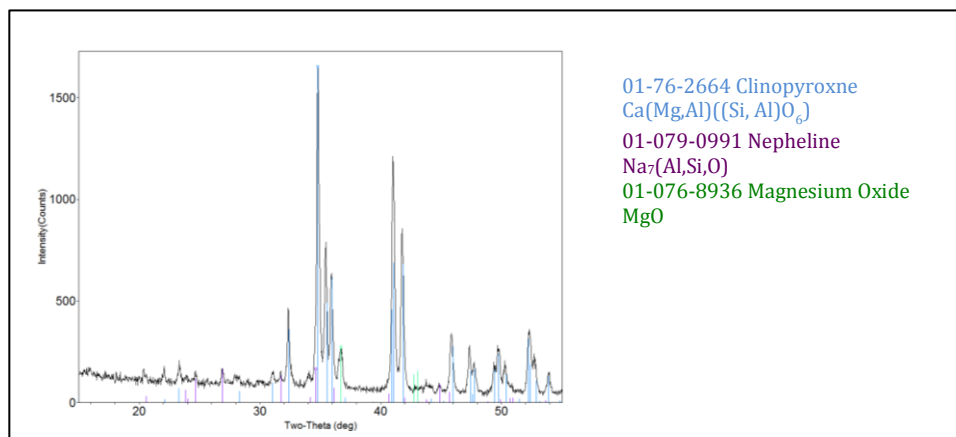


Figure 24. Phase ID of sample D after heat treatment.

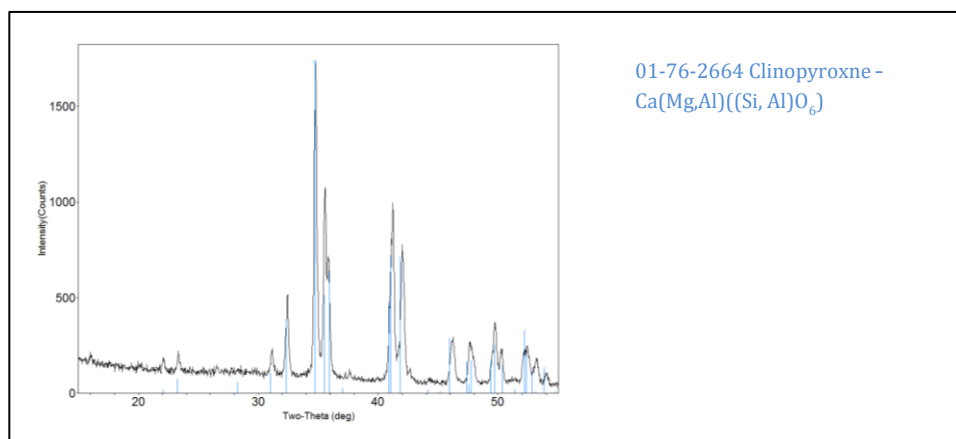


Figure 25. Phase ID of sample E after heat treatment.

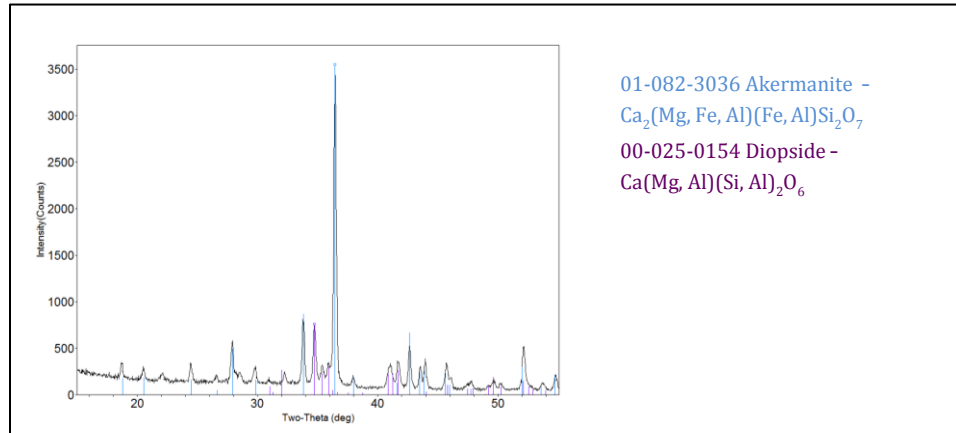


Figure 26. Phase ID of sample F after heat treatment (air).

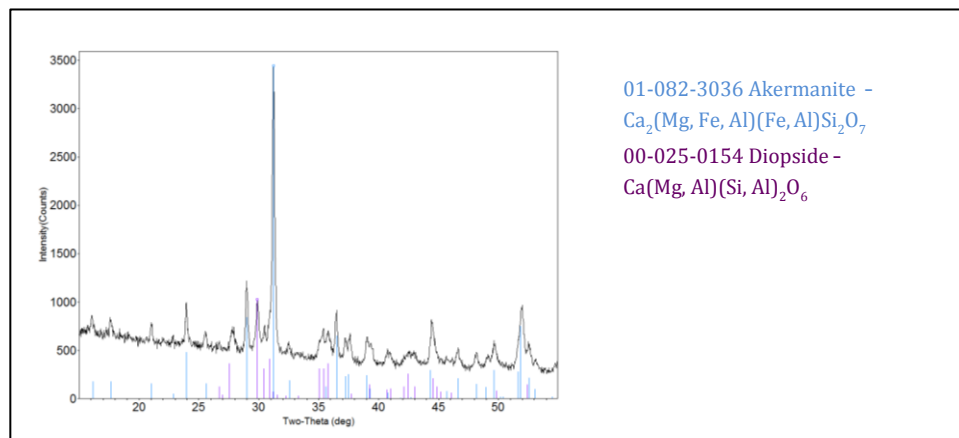


Figure 27. Phase ID of sample F after heat treatment (4%  $\text{H}_2$ ).

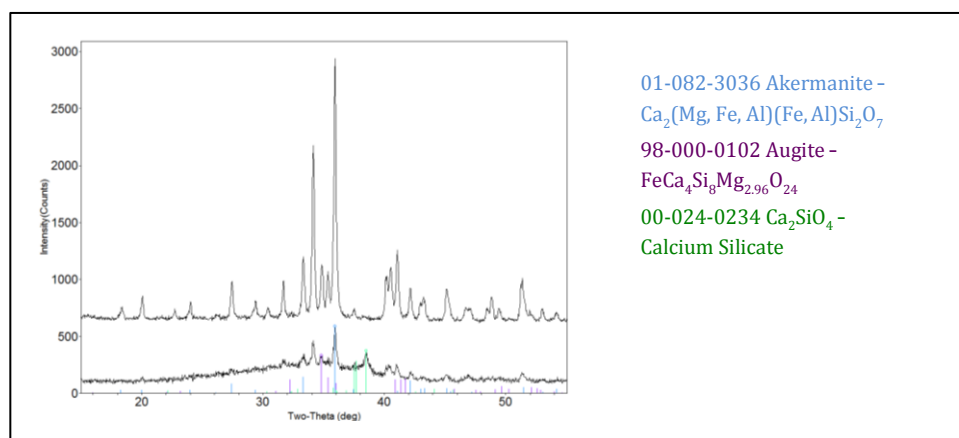


Figure 28. Phase ID of sample C at 820°C and 900°C illustrating how originally  $\text{Ca}_2\text{SiO}_4$  was present at 820°C, but faded out at 900°C.

### C. SEM

SEM was used to observe the origins of crystallization of these glass fibers. Fibers broken after heat treatment were analyzed, and it appeared as though crystallization occurred mostly on the surface. Examples of this can be seen in samples B, C, D, and F in figures 29-32 below. A broken fiber of sample A could not be found, and sample E was not analyzed in the SEM. The range of crystal sizes varied from sample to sample. A table of this can be seen in Table X (below).

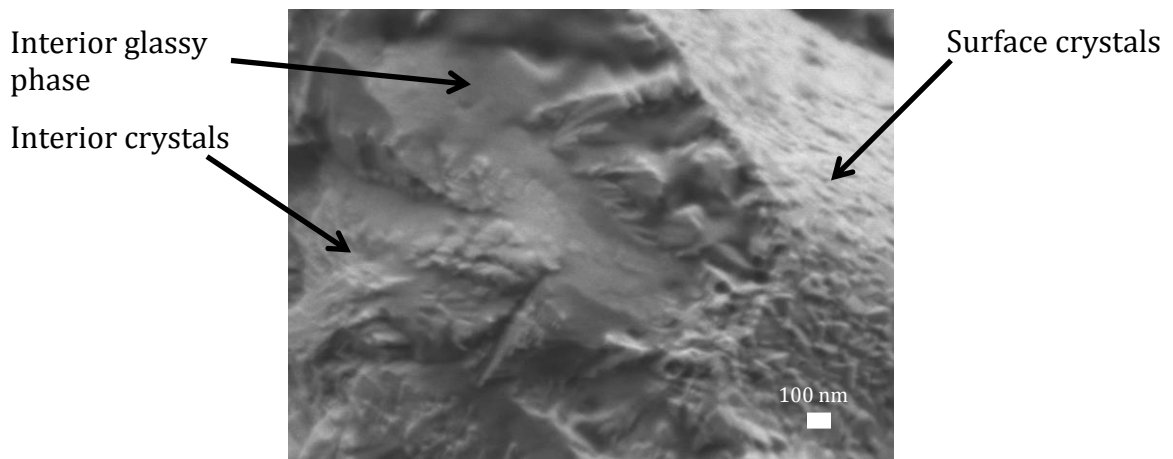


Figure 29. SE image of sample B heat treated at 800°C for 1 hr.

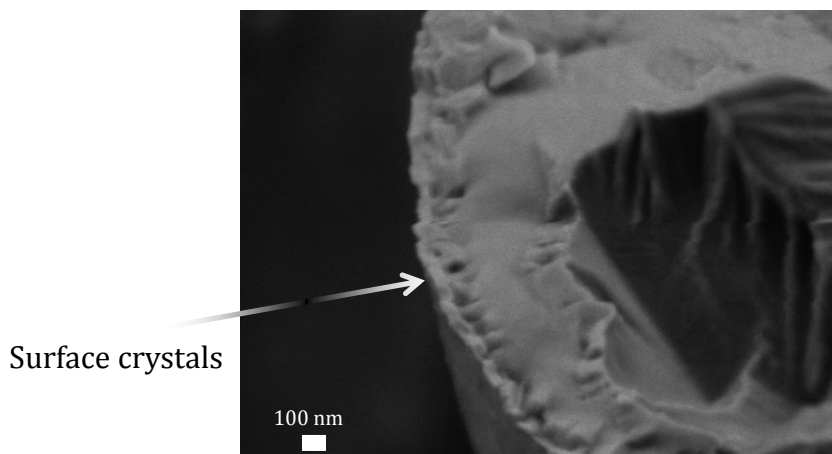
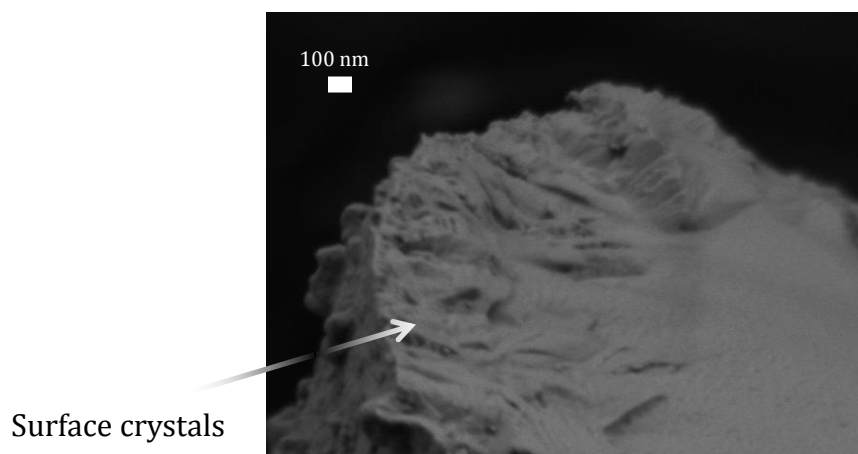
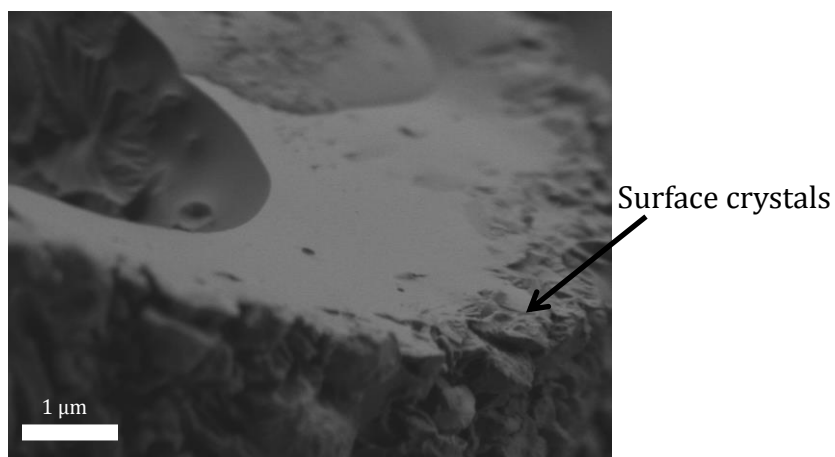


Figure 30. SE image of sample C heat treated at 800°C for 1 hr.



*Figure 31. SE image of sample D heat treated at 800°C for 1 hr.*



*Figure 32. SE image of sample F heat treated at 800°C for 1 hr.*

Unlike the HTXRD experiments, there was a difference in heat treatment in air compared to in the low oxygen atmosphere of the HTSEM. Minimal crystallization was observed when sample F was heat treated in the SEM, however when sample F was heat treated in air, very large and robust crystals were formed. This difference can be seen in figure 33 (below).

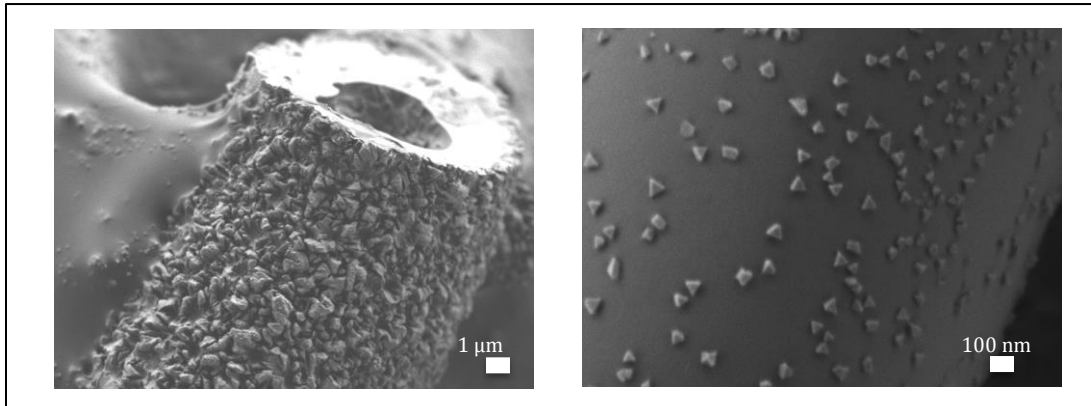


*Figure 33. SE images of sample F heated in air (left) and a low  $pO_2$  atmosphere (right).*

#### **D. XPS**

XPS was used to gain information about the oxidation states of iron before and after heat treatment. Sample A (high iron) and Sample F (low iron) were analyzed. Sample F contained too little iron to obtain information about oxidation states. Sample A, however contained enough iron to be analyzed. The binding energy of the FeO peak was approximately 710eV, while the binding energy for Fe<sub>2</sub>O<sub>3</sub> was approximately 724eV. The area ratio of the Fe<sup>3+</sup> to Fe<sup>2+</sup> peaks before heat treatment was 3.5., while the area ratio of the Fe<sup>3+</sup> to Fe<sup>2+</sup> peaks post heat treatment was 2.2. High resolution XPS scans of sample A pre and post heat treatment can be seen in figures 34 and 35 below.

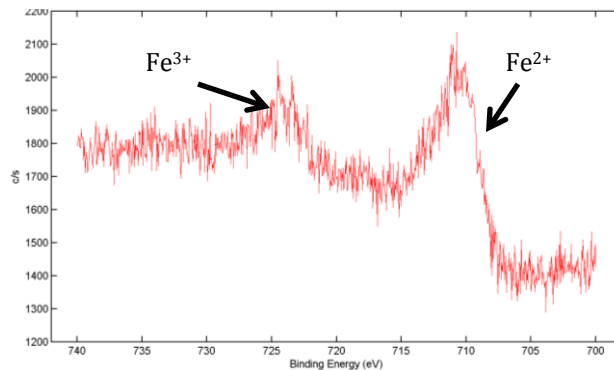


Figure 34. XPS scan of sample A pre heat treatment.

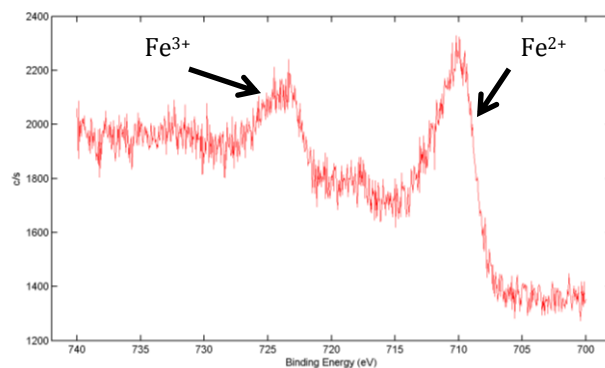


Figure 35. XPS scan of sample A post heat treatment.

## IV. Discussion

### A. HTXRD

As stated above, samples A, B, D, and E formed the phase clinopyroxene. These differed from samples C and F, which formed akermanite not by iron content, but by manufacturer. Samples C and F also contained a lower former to modifier ratio of 1.3. Akermanite is classified under the sorosilicates, which form silicon tetrahedral pairs, while clinopyroxene is classified under the inosilicates, which form chains of silicon tetrahedra. Samples C and F formed a sorosilicate because it had more modifier and modifiers tend to break up the glass network. Since samples A,

B, D, and E contained fewer modifiers they formed long chains of silicon tetrahedra (inosilicates).

As seen in the HTXRD plots and in the intensity of major peaks vs. temperature plot, sample A did not appear to crystallize as much as the other samples did. There was still an amorphous hump in the final HTXRD scan of sample A. Also in the final scan of sample A, the intensity of clinopyroxene reached just over 700 counts, where as in the rest of the samples the intensity was well into the thousands. This was surprising as sample A contained the most iron, therefore was expected to fully crystallize. As a result of the high iron content, sample A also had very small crystals. Small crystals can have a negative impact on the intensity of X-ray scans. Plots of peak intensity vs. temperature of samples A-E can be seen below in figures 36-40.

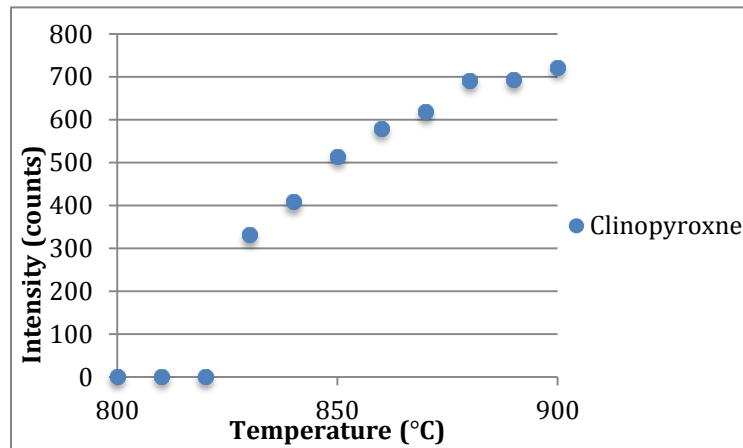


Figure 36. Sample A- Peak Intensity of Major Peak vs. Temperature.

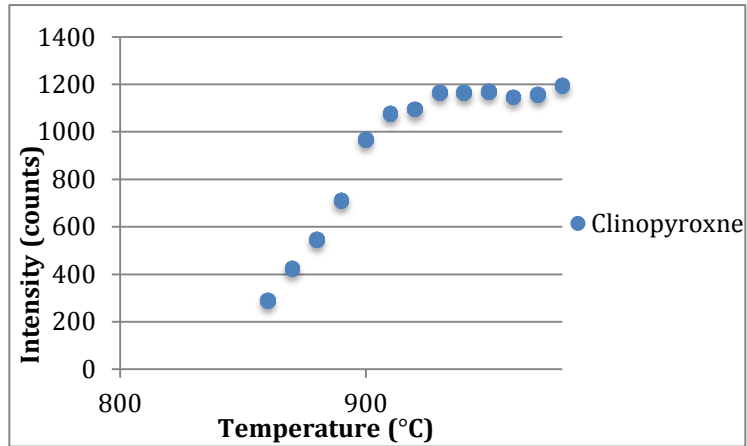


Figure 37. Sample B- Peak Intensity of Major Peak vs. Temperature.

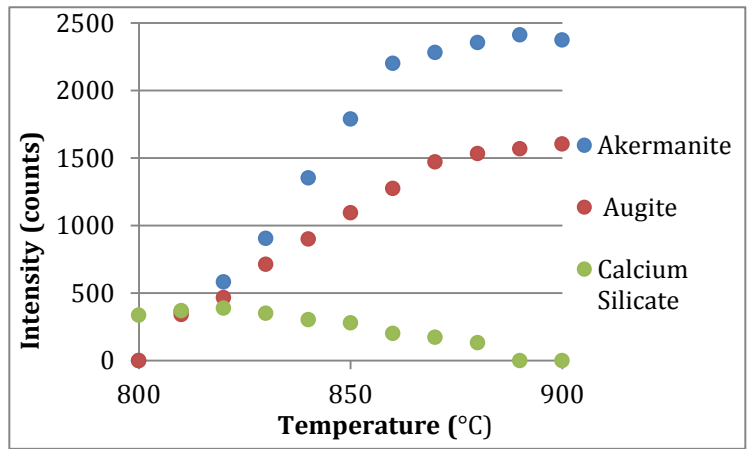


Figure 38. Sample C- Peak Intensity of Major Peaks vs. Temperature.

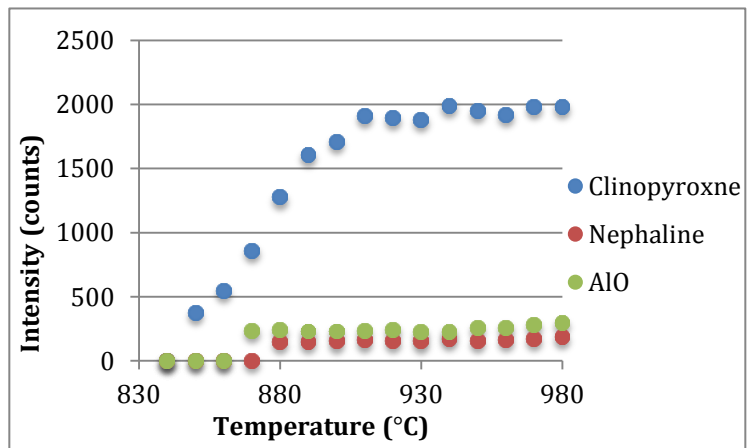


Figure 39. Sample D- Peak Intensity of Major Peaks vs. Temperature.

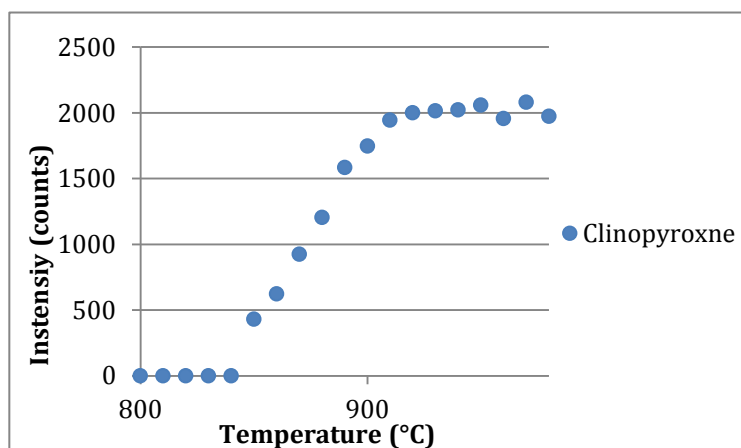


Figure 40. Sample E- Peak Intensity of Major Peak vs. Temperature.

Sample F was heat treated in both an ambient air atmosphere and a 4% H<sub>2</sub> reducing atmosphere. This had an unexpected effect on the way crystal phases formed. Both samples began crystallization at 840°C. At this temperature the intensity of the XRD peaks for the fibers heat treated in a reducing atmosphere was almost four times greater than those for the fibers heat treated in an oxygen-rich atmosphere. The fibers heat-treated under 4% H<sub>2</sub> reached maximum peak intensity at 860°C, while fibers in a high pO<sub>2</sub> atmosphere reached maximum peak intensity 10°C later at 870°C. Akermanite seemed to form slightly faster in the sample heat treated in the 4% H<sub>2</sub> atmosphere, however, temperatures could have varied in the furnace so this difference is not significant. This can be seen in figures 41 and 42 (below).

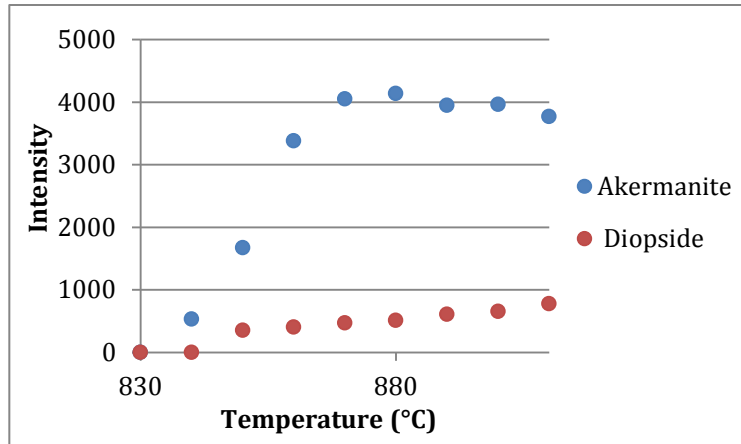


Figure 41. Sample F (air)- Intensity of Major Peak vs. Temperature.

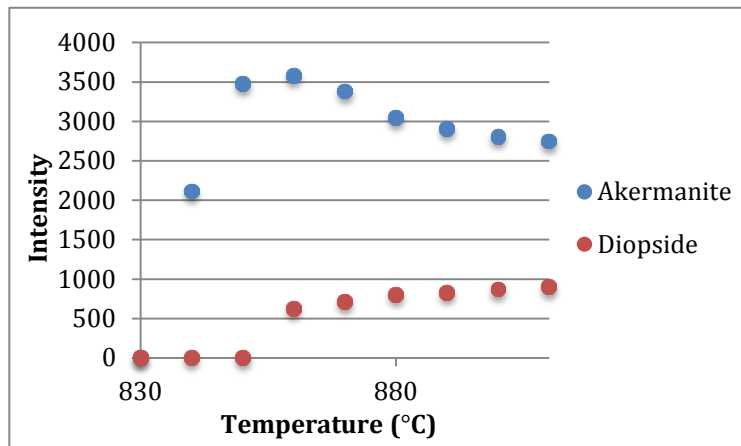


Figure 42. Sample F (4% H<sub>2</sub>)- Peak Intensity of Major Peak vs. Temperature.

## B. SEM

Samples with a lower iron content contained larger crystals, presumably from fewer nuclei. This trend was consistent across an iron content ranging from 2.65% to 17.32%. A plot of iron content vs. crystal size can be seen below in figure 43. The phases formed and former to modifier ratio did not have an effect on crystal size. A summary table of this can be seen in table XI. below.

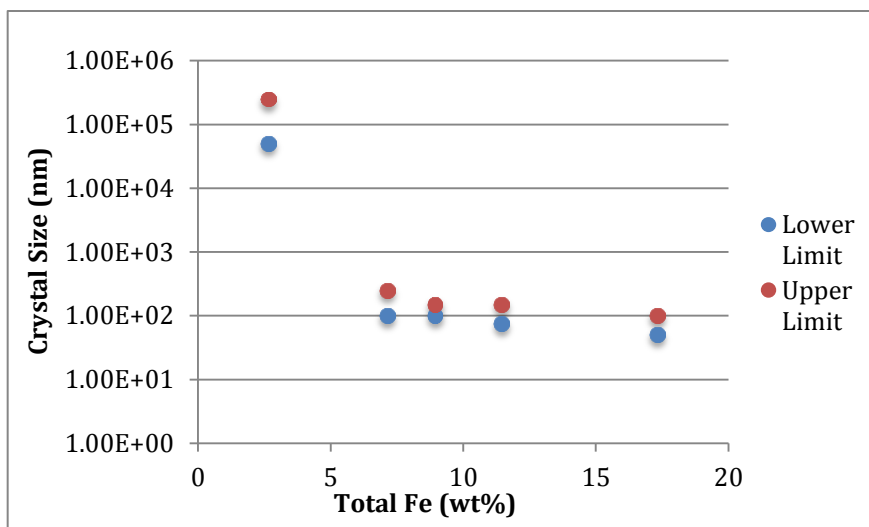


Figure 43. Iron content vs. crystal size.

Table XI. Summary Table

Sample	Total Fe (wt%)	Former to Modifier ratio	Crystal Size	Major Phase	Minor Phase(s)
A	17.32	2.9	50-100 nm	Clinopyroxne	None
B	11.45	2.9	75-150 nm	Clinopyroxne	None
C	8.93	1.3	100-150 nm	Akermanite	Augite Calcium Silicate
D	7.13	1.9	100-250 nm	Clinopyroxne	Nepheline Aluminum Oxide
E	7.08	1.7	N/A	Clinopyroxne	None
F	2.65	1.3	50-250 $\mu$ m	Akermanite	Diopside

Sample F contained the largest crystals when heat treated in air (800°C for 1 hour), however, when the same sample was heat treated in the low pO<sub>2</sub> atmosphere of the SEM at 825°C for over an hour, the crystallization was minimal. This result suggests that the atmospheric oxygen content has an effect on the way mineral wool fibers crystallize. The atmosphere controlled HTXRD experiments showed that the

akermanite phase probably crystallized faster under H<sub>2</sub> so the effects of pO<sub>2</sub> remain unclear.

### **C. XPS**

The FeO to Fe<sub>2</sub>O<sub>3</sub> area ratios pre and post heat treatment were 3.5 and 2.2 respectively. This suggests that the amount of divalent iron decreased after heat treatment, while the amount of trivalent iron increased, so the iron oxidized upon heat treatment.

## **V. Conclusions**

Several methods of characterization were carried out to study the crystallization of mineral wool. According to DSC, iron content played a role in determining the glass transition temperature, but not crystallization temperature. Samples with higher iron content had lower T<sub>g</sub>. The data collected from HTXRD showed that the glass former to glass modifier ratio had an impact on the crystalline phases formed. Samples with a lower former to modifier ratio formed akermanite, while samples with a higher ratio formed clinopyroxene. Akermanite is classified under the sorosilicates, which form silicon tetrahedral pairs, while clinopyroxene is classified under the inosilicates, which form chains of silicon tetrahedra. Samples with a lower former to modifier ratio formed a sorosilicate because it had more modifier and modifiers tend to break up the glass network. Samples with a higher former to modifier ratio contained fewer modifiers, so they formed long chains of silicon tetrahedra (inosilicates). The atmosphere in which the fibers were crystallized did not have an impact on the phases that formed, but did have a small

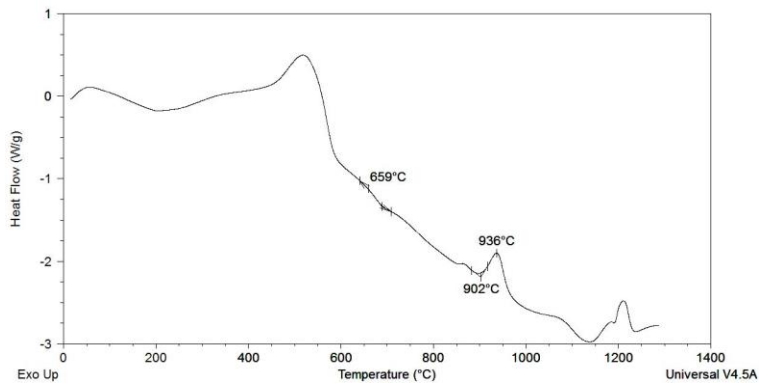
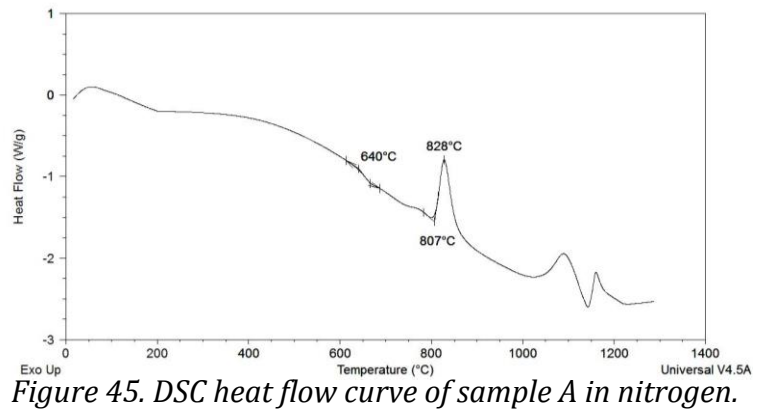
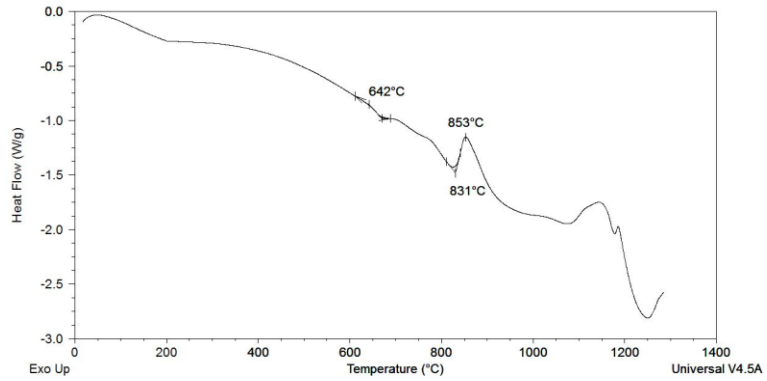
impact on crystallization kinetics according to HTXRD. SEM analysis proved that samples with lower iron content contained larger crystals, presumably from fewer nuclei. This trend was observed across an iron content ranging from 2.65 wt% to 17.32 wt%. Heat treatment inside of the low  $pO_2$  atmosphere of the HTSEM had an impact on the amount of crystal phase formed. Much smaller and fewer crystals were observed when fibers were heat treated in a reducing atmosphere when compared to an oxidizing atmosphere. Results from the XPS illustrated that the amount of  $Fe^{2+}$  decreased and  $Fe^{3+}$  increased upon heat treatment in air.

## **VI. Suggestions For Future Work**

In the future it would be of interest to look into the effect of different atmospheres on crystallization. This will help to give more information about the role iron oxidation states play in crystallization. The HTXRD and HTSEM did not 100% agree, so it would also be beneficial to look further into this.

## VII. Appendix

### A. DSC Heat Flow Curves



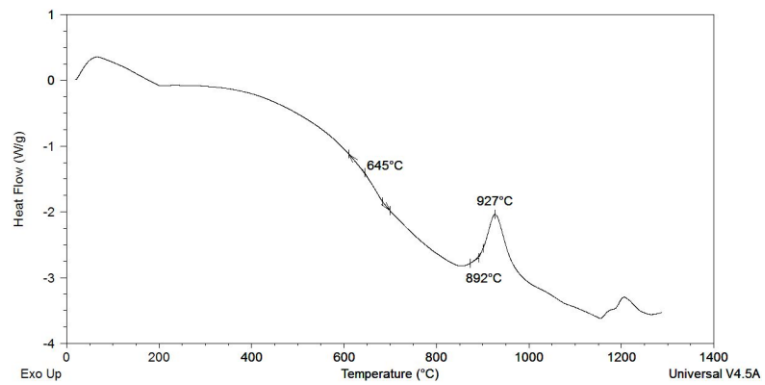


Figure 47. DSC heat flow curve of sample B in nitrogen.

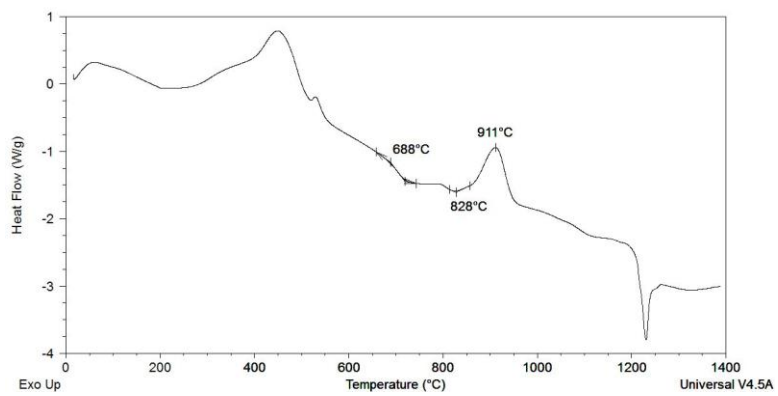


Figure 48. DSC heat flow curve of sample C in air.

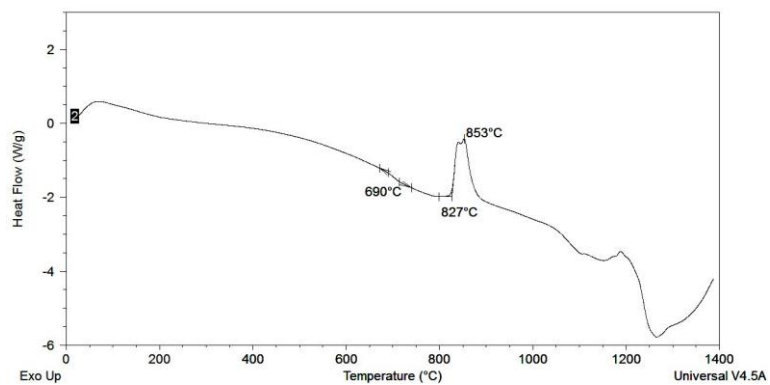
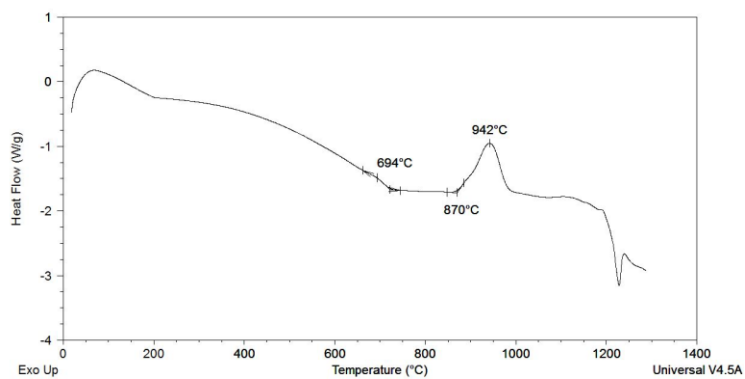
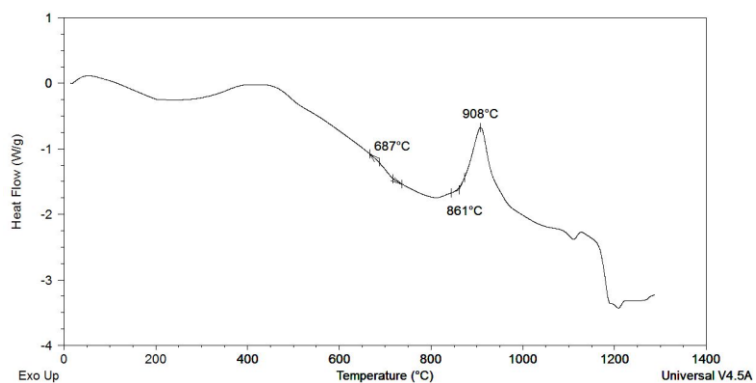


Figure 49. DSC heat flow curve of sample C in nitrogen.



*Figure 50. DSC heat flow curve of sample D in air.*



*Figure 51. DSC heat flow curve of sample D in nitrogen.*

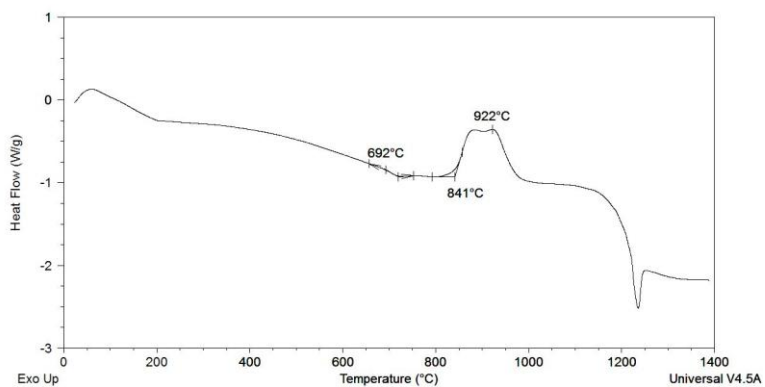


*Figure 52. DSC heat flow curve of sample E in air.*

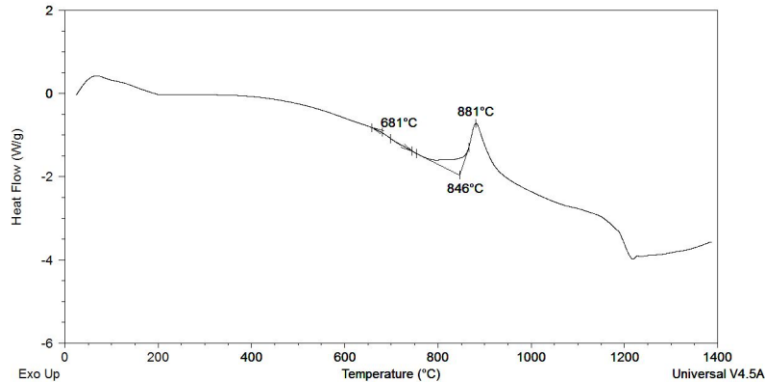


Figure 53. DSC heat flow curve of sample E in nitrogen.

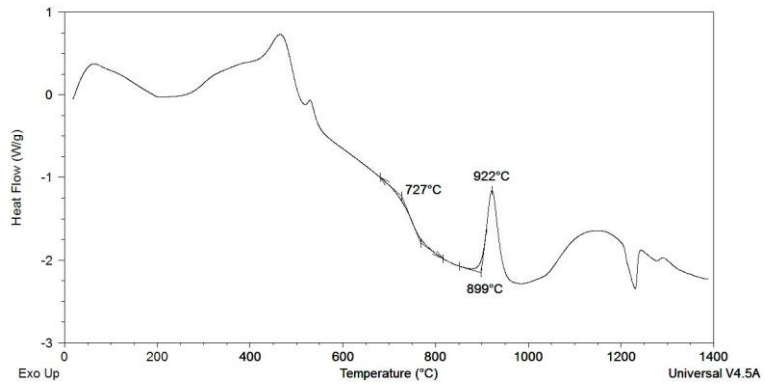


Figure 54. DSC heat flow curve of sample F in air.

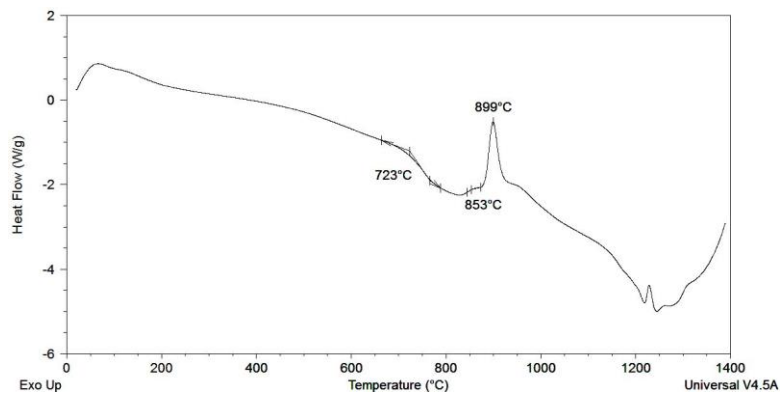


Figure 55. DSC heat flow curve of sample F in nitrogen.

## B. Additional SEM Images

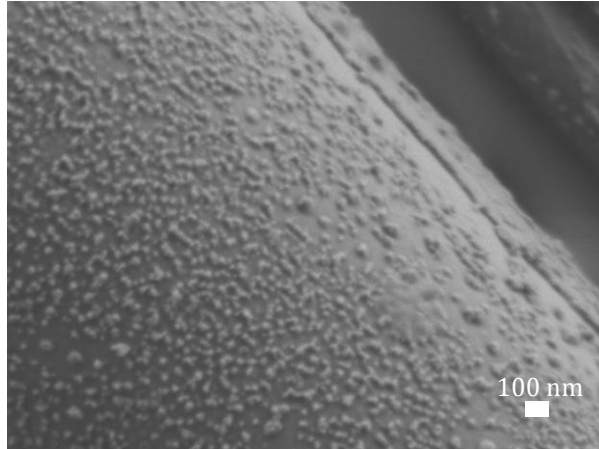


Figure 56. Sample A- pre heat treatment.

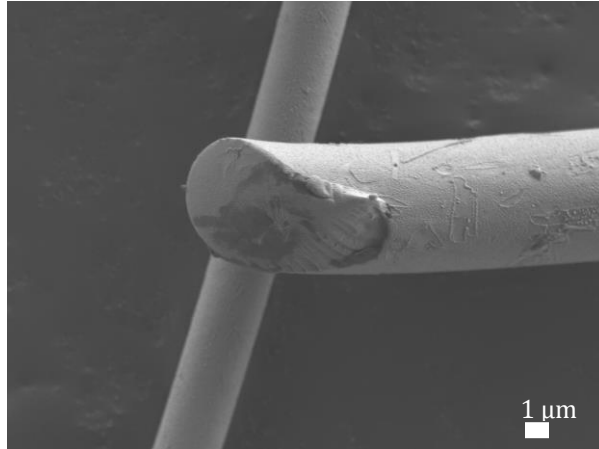


Figure 57. Sample A post heat treatment.

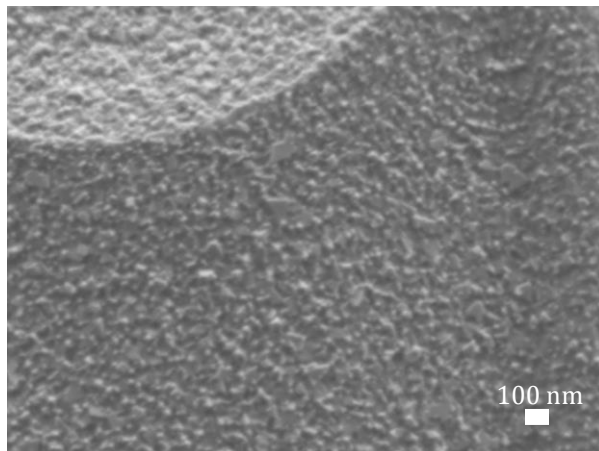
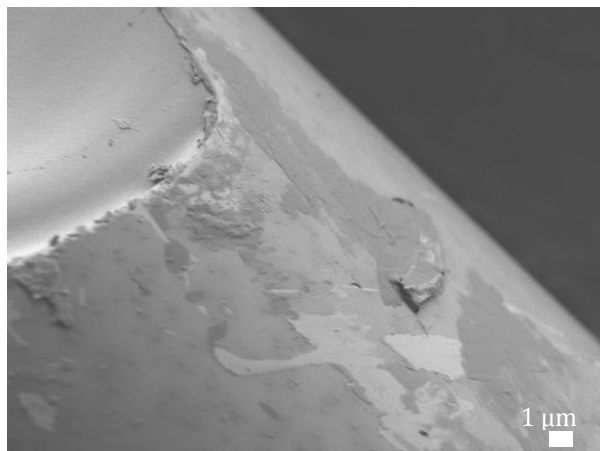
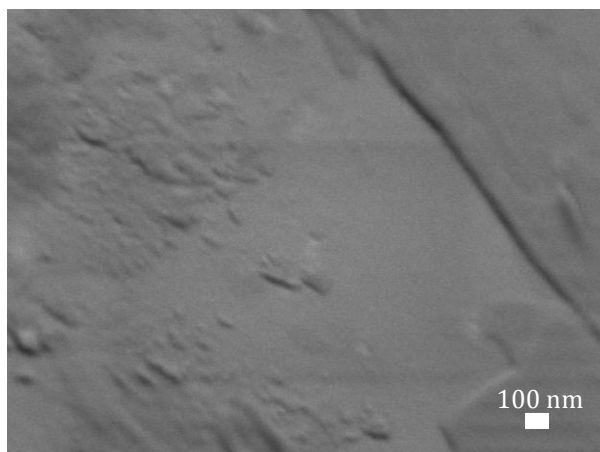


Figure 58. Sample A post heat treatment.



*Figure 59. Sample B pre heat treatment.*



*Figure 60. Sample B pre heat treatment.*

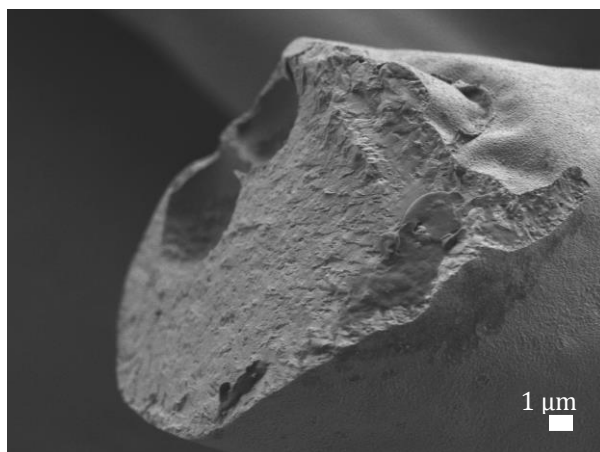


*Figure 61. Sample B fiber that broke after heat treatment.*

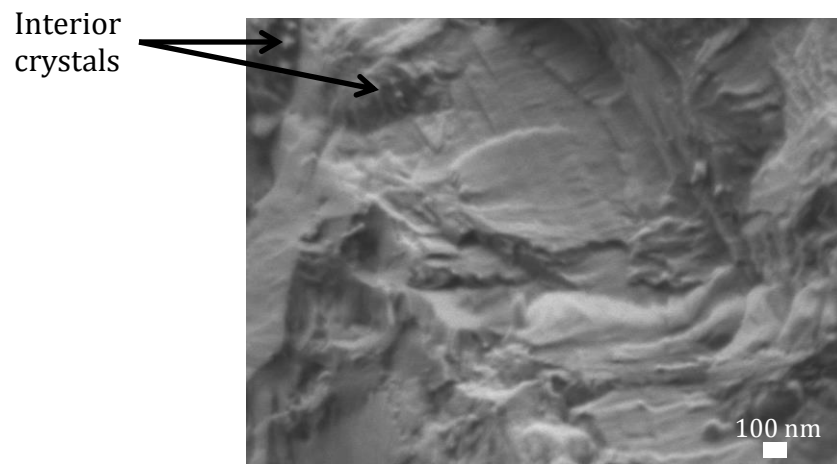


*Figure 62. Sample B post heat treatment.*

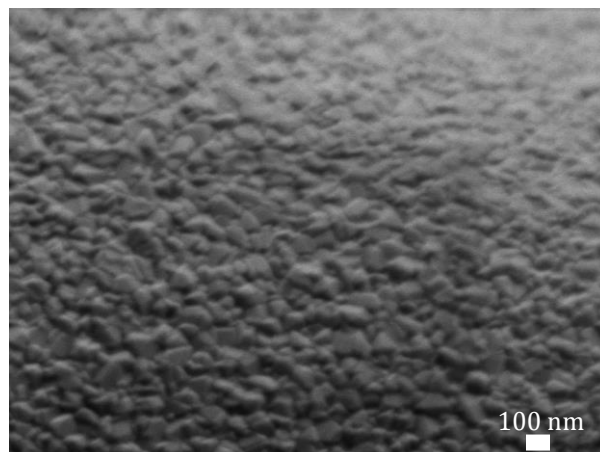


*Figure 63. Sample B surface crystallization post heat treatment.*

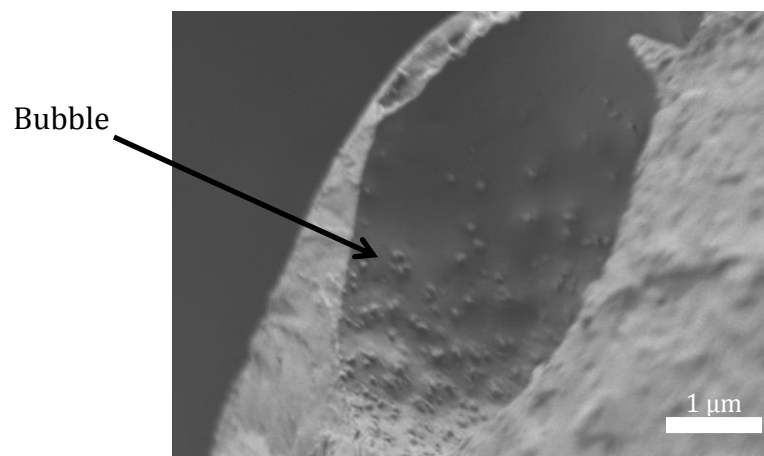


*Figure 64. Sample B post heat treatment.*

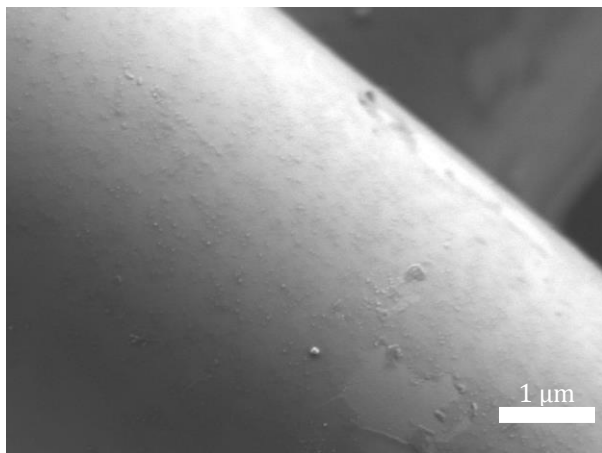


*Figure 65. Sample C pre heat treatment.*

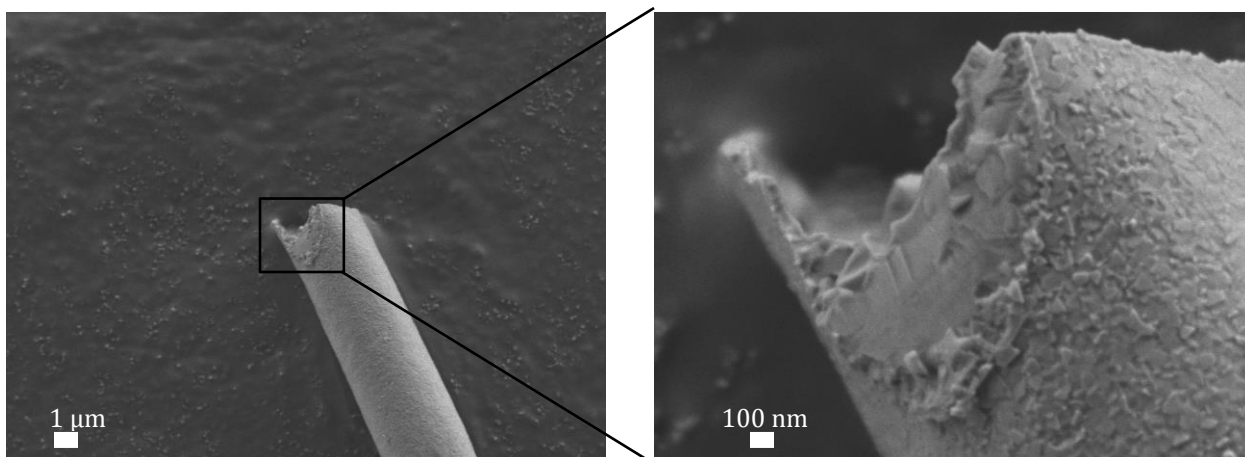


*Figure 66. Sample C fiber that chipped post heat treatment.*

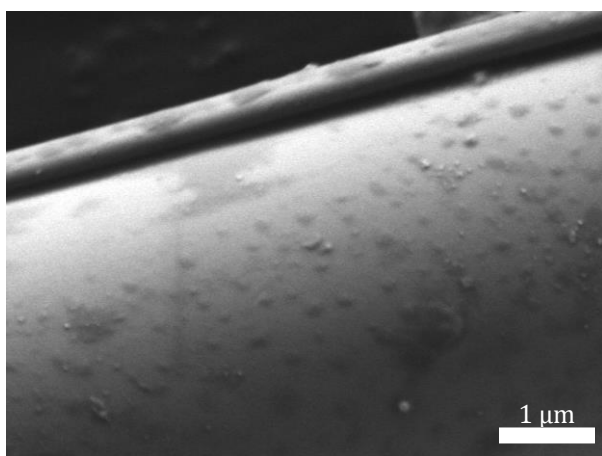


*Figure 67. Sample D pre heat treatment.*

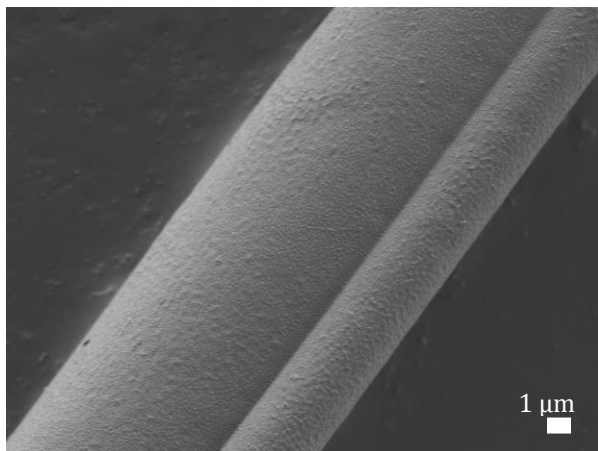


*Figure 68. Sample D post heat treatment.*

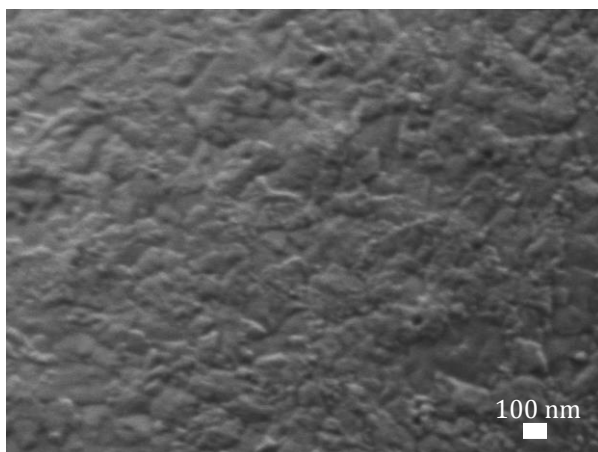


*Figure 69. Sample D post heat treatment crystalline surface.*

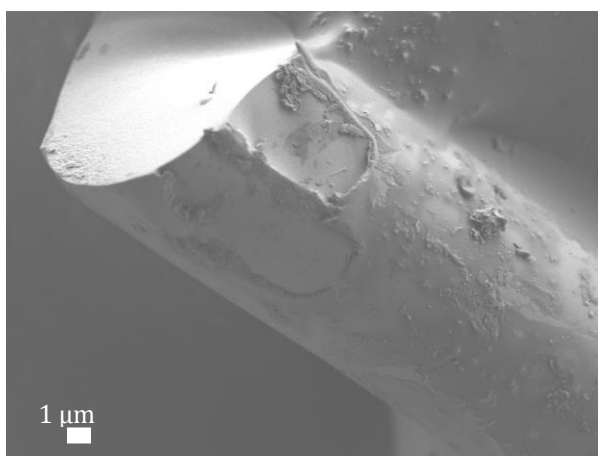


*Figure 70. Sample F pre heat treatment (air).*

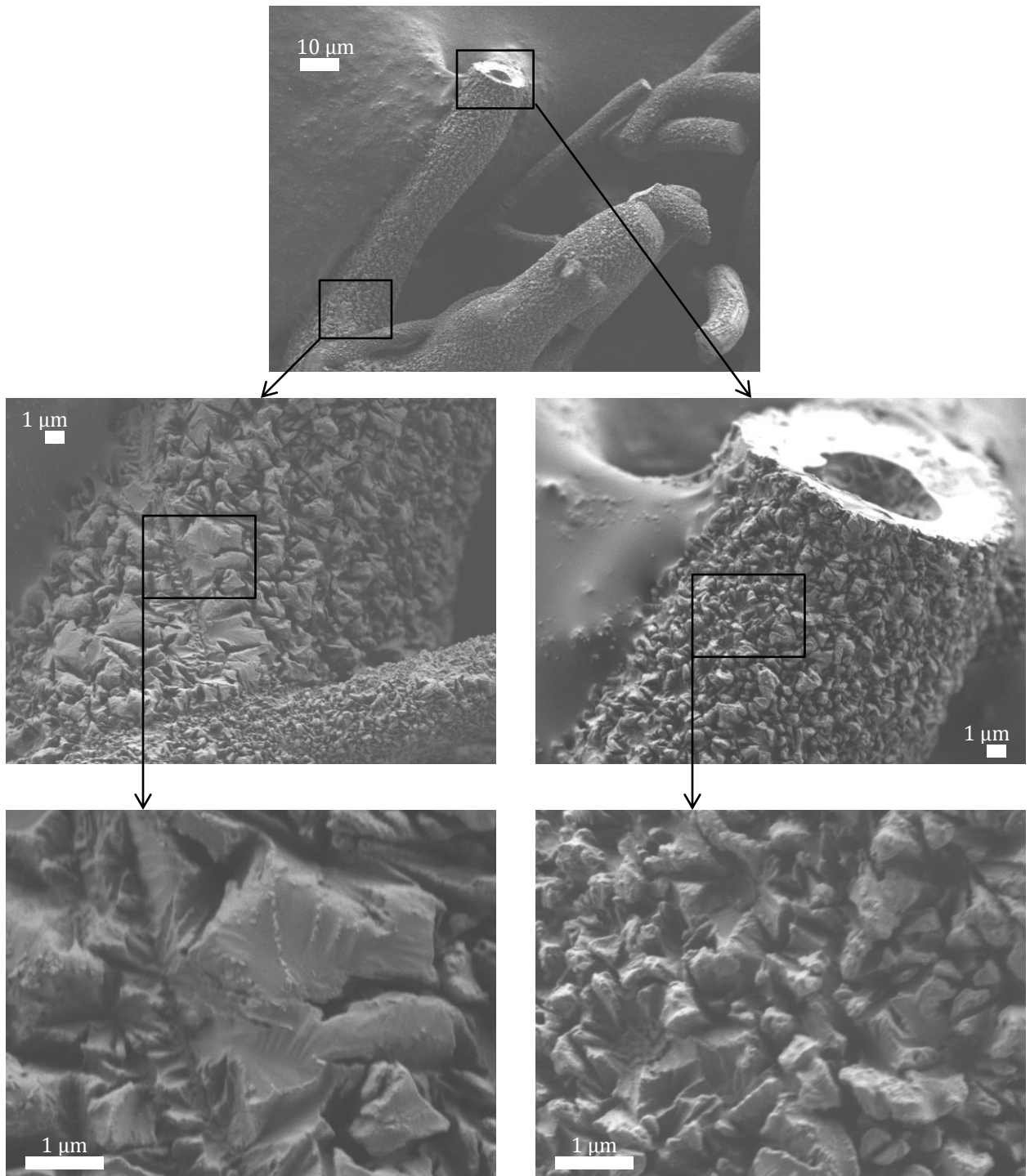
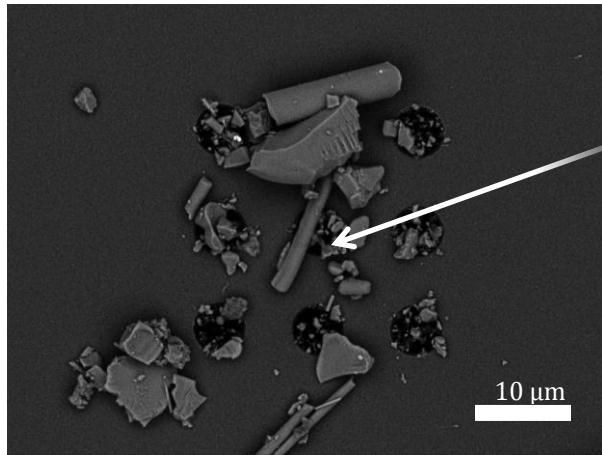


*Figure 71. Sample F post heat treatment (air).*



Fiber  
examined  
during heat-  
treatment

*Figure 72. Sample F post heat-treatment (low  $pO_2$ ).*

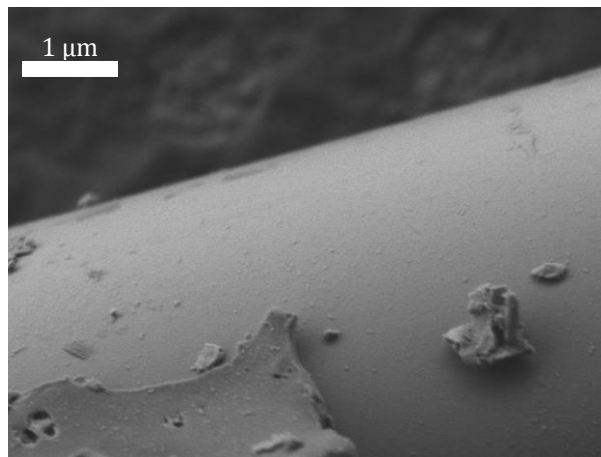


*Figure 73. Sample F pre heat-treatment (low  $pO_2$ ).*

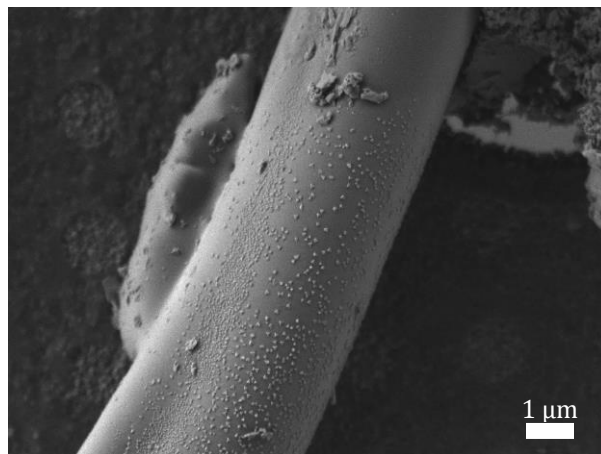


*Figure 74. Sample F post heat-treatment (low  $pO_2$ ).*

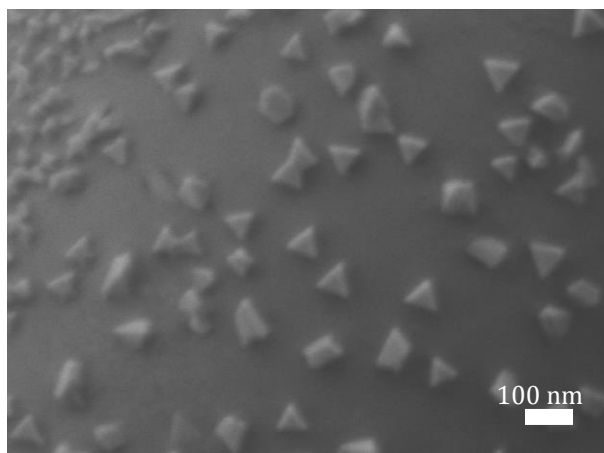


*Figure 75. Sample F post heat-treatment (low  $pO_2$ ).*

## VIII. References

1. W. Holand and G.H. Beall, *Glass-Ceramic Technology*, 2<sup>nd</sup> ed.; **pp.** xvii & 1-9. John Wiley & Sons Inc., Hoboken, NJ, 2012.
2. R.D. Rawlings, J.P. Wu and A.R. Boccacchi, "Glass-ceramics: Their production from wastes- A Review," *J. Mater. Sci.*, **41** 733-761 (2006).
3. B. Roy, "Glass-wool Insulation: ECBC Compliance and Green Building Aspect," *Key Eng.r Matls.*, **632** 39-44 (2015).
4. N. Lonroth, C.L. Muhlstein, C. Pantano, Y. Yue, "Nanoindentation of glass wool fibers," *J. Non-Cryst. Solids*, **354** 3887-3895 (2008).
5. A.A. Alarifi, J. Dave, H.N. Phylaktou, O.A. Aljumaiah and G.E. Andrews, "Effects of fire-fighting on a fully developed compartment fire: Temperatures and emissions," *Fire Safety J.*, **68** 71-80 (2014).
6. T. Tian, Y. Zhang, A. Yang, Z. Zhang, "Crystallization Behavior and Damage Mechanism of Mineral Wool Fibers When Heated," Tech. Rept. 0.1007/s12666-016-0959-8, The Indian Institute of Metals, Sept. 2016.
7. M.M. Smedskjaer, M. Slovang, Y. Yue, "Crystallization behavior and high-temperature stability of stone wool fibers," *J. European. Ceram. Soc.*, **30** 1287-1295 (2010).
8. A. Karamanov, P. Pisciella, C. Cantalini and M. Pelino, "Influence of Fe<sup>3+</sup>/Fe<sup>2+</sup> Ratio on the Crystallization of Iron-Rich Glasses Made with Industrial Wastes," *J. Am. Ceram. Soc.*, **83** [12] 3153-3157 (2000).
9. X. Yongli, L. Yin and L. Yongquian, "Status and development of mineral wool made from molten blast furnace slag," *Baosteel Tech. Research*, 5 [2] 3-8 (2011).
10. M. Moesgaard, H.D. Pedersen, Y.Z. Yue E.R. Nielsen, "Crystallization in stone wool fibers," *J. Non-Cryst. Solids*, **393** 1101-1108 (2007).
11. S.T. Mixture, "Large-Volume Atmosphere-Controlled Diffraction Furnace," *Measurement Sci. and Tech.* 14 1091-1098 (2003).